Polo-like kinase 1 regulates growth in juvenile *Fasciola hepatica*

[1]Paul McCusker¶*, [1]Nathan G. Clarke¶, [1]Rebecca Armstrong, [1]Duncan Wells, [1]Emily Robb, [1]Paul McVeigh, [2]Andreas Krasky, [3]John Harrington, [2]Paul M. Selzer, [1]Nikki J. Marks, [1]Aaron G. Maule*

1. Understanding Health & Disease, School of Biological Sciences, Queen's University Belfast, Belfast BT9 5DL, UK
2. Boehringer Ingelheim Animal Health, Binger Str. 173, 55216 Ingelheim am Rhein, Germany
3. Boehringer Ingelheim Animal Health, 1730 Olympic Dr, Athens, GA 30601, USA

*Corresponding Authors

Email: pmccusker09@qub.ac.uk (PMcC)

Email: a.maule@qub.ac.uk (AGM)

¶These authors contributed equally to this work

Abstract

Fasciola sp. (liver fluke) are parasitic flatworms that impose a significant burden on the agri-food industry and human health. Immature worms can cause severe damage to the liver as they migrate towards the bile ducts, and yet there is only a single drug to treat this pathogenic life stage, driving the need to identify targets for novel flukicides. Given their crucial role in the growth/development of immature *Fasciola hepatica*, neoblast-like stem cells are an attractive source of new flukicide targets. Kinases are a hugely diverse group of phosphorylating enzymes with key roles in almost all cellular processes. Kinase dysregulation can result in the development of cancerous cells/tissues, linking many to cell cycle-associated proliferation and growth. Here, we annotate the *F. hepatica* kinome, identifying 271 putative protein kinases, representing around 1.6% of predicted *F. hepatica* protein-coding genes with family proportions similar to those of other parasitic flatworms. Many of these kinases, such as polo-like kinase 1 (*fhplk1*), are upregulated in immature worms undergoing rapid growth and development, a process underpinned by the proliferation of neoblast-like stem cells. RNA interference (RNAi)-mediated silencing of *fhplk1* in juvenile liver fluke reduced growth and cell proliferation, suggesting a conserved role within the cell-cycle; the cessation of stem cell proliferation persisted for at least a week following *fhplk1*-RNAi. A PLK inhibitor (BI 2536) was shown to phenocopy the *fhplk1*-RNAi phenotype in a dose-dependent manner, supporting the feasibility of targeting *F. hepatica* neoblast-like cells through kinase inhibitors. Transcriptomic analysis of *fhplk1*-RNAi juveniles revealed 946 downregulated genes, principally associated with the cell cycle or ribosomes. Over 80 of these downregulated genes were also downregulated following juvenile *F. hepatica* irradiation, supporting roles for these kinases in neoblast-like stem cells, and marking them as putative targets for control. Among the 1244 upregulated genes in *fhplk1*-RNAi juvenile worms were many neurotransmitters, receptors and ion channels, exposing the apparent upregulation of diverse inter-cellular signalling systems. While many neurotransmitter pathways promote proliferation in mammalian systems the interaction between neoblast-like stem cells and neuronal signalling in parasitic flatworms remains elusive. Here, the transcriptomic response of *fhplk1*-RNAi juveniles supports a link between neoblast-like stem cell driven growth/development and neuronal signalling.

Author Summary

The liver fluke is a parasitic flatworm which causes disease in livestock and humans around the world. While establishing the infection, immature liver fluke migrate through the host liver causing significant damage. Unfortunately, only one drug is currently recommended for treatment of these immature worms, though resistance to this drug is now widespread and exposes the pressing need to develop novel drugs. As worms migrate through the liver, they undergo growth and development which is facilitated by proliferating stem cells. These neoblast-like cells are akin to stem cells seen in other organisms, and as such are responsible for new tissue growth. Many stem cells express kinases, a large family of enzymes that control many cellular processes. In this study we identified all the potential kinases in the liver fluke, including those that may function in neoblast-like stem cells. One of these kinases, polo-like kinase 1 (PLK1), has been linked to cancer development in humans. We used reverse genetics to silence this gene, allowing us to understand its function. Silencing PLK1 reduced worm growth and stopped neoblast-like cell proliferation, confirming that it has an important role in growth and cell division. Also, we showed that a PLK1 inhibitor, developed for cancer treatments, reduced growth and neoblast-like cell activity, illustrating the potential for targeting liver fluke kinases associated with neoblast-like cells with drugs, providing new routes to drug development. We then carried out RNA sequencing of worms after PLK1 was silenced to show the effects of neoblast-like cell loss on the expression of other genes. We found a decrease in the expression of genes that regulate cell division, but an increase in the expression of genes related to inter-cell signalling, including neuronal genes. This supports evidence for interactions between the nervous system and neoblast-like cells which could be exploited in future drug discovery.

Introduction

Infections with the trematode parasite, *Fasciola hepatica*, can lead to fasciolosis, which is estimated to cause >$3 billion in losses to global livestock yield every year [1]. It also poses a significant threat to human health as a neglected tropical disease [2]. Reports of frontline flukicide (triclabendazole, TCBZ) treatment failure in sheep, cattle and human infections [3], encourage the search for new flukicides, an activity underpinned by novel drug target discovery and validation [4]. This is necessary as TCBZ is uniquely effective in combatting the migrating, highly pathogenic, juvenile parasites which cause the acute stage of the disease. Furthermore, despite intensive research we do not fully understand the mechanisms of TCBZ action or resistance [3,5,6].

Identification of novel targets that disrupt juvenile *F. hepatica* growth/development could underwrite future control programs. Growth in the related free-living flatworms is driven by neoblasts, somatic stem cells that endow species like *Schmidtea mediterranea* with remarkable regenerative capabilities [7]. These neoblasts are sensitive to irradiation [8], and intriguingly, early attempts to develop *F. hepatica* vaccines with irradiated metacercariae restricted development in a mammalian host [9,10]. If this stunted growth in irradiated *F. hepatica* metacercariae was due to disruption of a neoblast-like cell population, it encourages exploration of neoblast-like cells as targets for future flukicides. Over the last decade a range of studies have identified how proliferating stem cells in several parasitic flatworms, including *Schistosoma mansoni*, *Echinococcus multilocularis* and *Hymenolepis diminuta*, facilitate parasite development and tissue renewal/repair, potentially enabling long-term parasitism within hostile host environments [11–19]. Development of an *in vitro* culture platform for juvenile *F. hepatica* enables juveniles to grow/develop towards an adult-like phenotype and showed that *F. hepatica* growth/development was supported by proliferation of neoblast-like stem cells [20]. Furthermore, a recent study demonstrated that irradiation ablates the neoblast-like cell population of *F. hepatica*, resulting in downregulation of stem cell associated transcripts [21].

Numerous protein kinases (PKs) are associated with proliferating cells. PKs are a diverse group of phospho-transferase enzymes that facilitate transfer of the γ-phosphate on an ATP to a substrate's hydroxyl-group [22]. The human kinome comprises more than 500 PKs [23] that play crucial roles in nearly every aspect of cell biology, with studies suggesting that up to 90% of expressed proteins may be phosphorylated [24]. Functional PKs are typically classed into two groups, the eukaryotic protein

99 kinases (ePKs) and the atypical protein kinases (aPKs) [23]. A staggering 85% of PKs have been linked
100 to cancer or other diseases/developmental disorders [25]. It's unsurprising therefore that there has been
101 intense development of kinase inhibitors over the last 20 years [26], with over 400 currently in clinical
102 trials (https://www.icoa.fr/pkidb/). The critical role of PKs in many cellular processes, and the abundance
103 of kinase inhibitors make their interrogation as putative anthelmintic targets attractive. Indeed, a protein
104 kinase C-β inhibitor (ruboxistaurin) was shown to kill adult *F. hepatica in vitro* [27]. Kinomes have been
105 assembled for several parasitic flatworms, *S. mansoni*, *Schistosoma haematobium* and *Taenia solium*
106 [28–31], illustrating that all nine major PK families are present, and that the kinome represents a similar
107 proportion of the proteome (1.8-1.9%) to that seen in other eukaryotes [23].

108 The active role of many PKs in the cell cycle/cell division means that mutations or dysregulation can
109 result in cancerous growths [32]. One set of PKs closely associated with the cell cycle are the polo-like
110 kinases (PLKs), named after a mutant form of the *polo* gene which prevented formation of functional
111 spindle poles during cell division in *Drosophila melanogaster* [33,34]. Additional PLKs have been
112 identified throughout the eukaryotes, from yeasts to humans [35–37], where they are implicated in
113 driving cell-cycle progression [38]. PLKs are serine/threonine kinases with a highly conserved domain
114 architecture, comprising an N-terminal kinase domain and a unique, C-terminal polo-box domain that
115 determines subcellular localisation, and is involved in autoinhibitory regulation of the kinase domain
116 [38]. Some organisms only encode a single PLK (e.g. yeast sp.), whereas others possess up to five
117 PLKs, as in humans [38].

118 Human PLKs1-3 possess a typical PLK conformation, while PLK4 is more divergent and PLK5 lacks an
119 active kinase domain [38]. Polo-like kinase 1 (PLK1) is most akin to *D. melanogaster polo*, with roles in
120 regulating cell cycle progression from the G2/M transition through to cytokinesis. PLK1 promotes mitosis
121 onset through phosphorylation of substrates that allow downstream activation of the cyclin-dependent
122 kinase 1 (CDK1) – cyclin B complex, driving cell entry into M-phase [29,30]. Other roles for PLK1 include
123 promoting disassembly of the interphase centrosome, formation of mitotic spindle, bipolar attachment
124 of microtubules to sister chromatids, anaphase progression and formation of the contractile ring
125 apparatus for cytokinesis [38,39]. PLK1 has also regularly been observed to be overexpressed in cancer
126 tissues, resulting in its appeal as a putative target for cancer therapies [39].

127 PLK1 has been linked to cell division in *S. mansoni* and *E. multilocularis* [40–43]. PLK inhibition in adult
128 schistosomes reduced gamete production as well as the viability of adults and schistosomula *in vitro*
129 [40,42]. Inhibiting PLK activity in *E. multilocularis* prevented cell proliferation in mature metacestodes
130 and rendered germinative cells unable to form metacestode vesicles *in vitro* [43]. These investigations
131 suggest that targeting PLK activity could represent a broad-acting anti-parasitic flatworm strategy. A
132 gene displaying typical PLK1 domain architecture has been reported in *F. hepatica* (FhPLK1, [44]) and
133 treatment of *ex vivo* immature and adult *F. hepatica* with the PLK1 inhibitor BI 2536 reduced motility
134 and limited adult egg production [45]. Furthermore, recent transcriptomic studies have linked the *F.*
135 *hepatica plk1* gene, *fhplk1*, with the neoblast-like proliferative cells of *F. hepatica* as it is upregulated in
136 faster-growing worms [46], and downregulated in worms with ablated neoblast-like cells [21].

137 Here, we have interrogated available *F. hepatica* genomic datasets to generate a *F. hepatica* kinome,
138 identifying 271 putative PKs. Furthermore, we demonstrate that RNA interference (RNAi) of *fhplk1*
139 undermines the neoblast-like cell driven growth of *in vitro*-cultured juveniles. Transcriptomics of *fhplk1*-
140 RNAi worms highlighted downregulation of many cell cycle effectors, alongside upregulation of inter-
141 cell signalling pathways. Additionally, we show that treating juvenile *F. hepatica* with the PLK1 inhibitor
142 BI 2536 *in vitro* phenocopies the effects of *fhplk1*-RNAi by disrupting neoblast-like cell driven growth.
143 Together, these data support the view that FhPLK1 has a conserved role as a cell cycle regulator in *F.*
144 *hepatica*, enhancing its drug target candidature as a means of disrupting *F. hepatica*
145 growth/development. Furthermore, our transcriptomic datasets facilitate identification of additional drug
146 target candidates and promote our understanding of interplay between *F. hepatica* neoblast-like cells
147 and other tissues.

148 # Results and Discussion

149 ## The *F. hepatica* kinome

150 Our bioinformatic screen (S1A Fig) of available *F. hepatica* genomes has enabled us to generate a
151 putative *F. hepatica* kinome. In total, 271 PKs were identified (S2 Table; S1 File) with 254 ePKs and 17
152 aPKs. This constitutes ~1.6% of the predicted *F. hepatica* proteome, a little smaller than the 1.8-1.9%
153 seen in *H. sapiens*, *S. mansoni*, *S. haematobium* and *T. solium* [23,28–30]. This could be due to the
154 large size of the *F. hepatica* genome, relative to other pathogens [47], or the incomplete nature of the
155 genome assembly, as the total number of PKs identified is comparable to that of *S. haematobium* (269,
156 [30]) and *S. mansoni* (253; updated genome assemblies have removed putative PKs since Grevelding
157 et al. [28]). BLAST searches revealed that 208/253 predicted *S. mansoni* kinase genes had a matching
158 hit in our *F. hepatica* kinome. Members of all nine ePK families were represented, with
159 calcium/calmodulin-dependent protein kinase (CAMK) and CMGC families found to be the largest
160 (Fig1A), representing around 30% of all ePKs. These proportions are similar to those of other parasitic
161 helminths, such as *T. solium, Schistosoma* spp., *B. malayi* and *H. contortus* (S1B Fig; [28–31,62,63]).
162 This contrasts with free-living species (*C. elegans*, *D. melanogaster* and humans), where tyrosine
163 kinases (TK) are the largest family (S1B Fig; [23,48,49]), suggesting a reduced role of TKs in parasitism.
164 We also noted a contrast between the kinomes of ecdysozoans and lophotrochozoans/deuterostomes
165 (S1B Fig), with an expansion of the casein kinase I (CK1s) and receptor guanylate cyclase (RGCs)
166 families in the ecdysozoans, potentially indicating roles for CK1 and RGC in the regulation of moulting.

167

168 **Fig 1. *Fasciola hepatica* kinases are enriched in developing life stages.**
169 (A) CLANs analysis (1M iterations) of *F. hepatica* eukaryotic protein kinases shows presence of all nine
170 major families with conservation among CMGC kinases and mitogen-activated protein kinases (STEs)
171 but divergence among tyrosine kinase-like kinases (TKLs), casein kinases (CKs) and
172 calcium/calmodulin kinases (CAMKs). (B) Heatmap of *F. hepatica* kinases (where data was available)
173 in various life stages (Left) with average euclidean distancing applied shows upregulation of many
174 kinases in newly excysted juveniles (NEJs) and immature worms as well as upregulation of the majority

175 of kinases in *in vivo* juveniles compared to *in vitro* juveniles (Right), colours correspond to z scores (red
176 = upregulated; blue = downregulated; grey = no change; black = no expression data).

177

178 The largest *F. hepatica* ePK family (CAMK) contains both substrate restricted and multifunctional
179 kinases with a range of homeostatic roles [50]. Due to their critical roles in Ca^{2+} signalling pathways,
180 they have been proposed as potential anthelmintic targets. Schistosome CAMKII increases its
181 expression/activity following treatment with the paralysis-inducing drug praziquantel, with RNAi
182 reducing motility/viability [51,52], suggesting that CAMKII plays a role in worm motor function/motility.
183 The CMGC family is the second largest ePK family in *F. hepatica.* This highly conserved family consists
184 of members that play critical roles in cell cycle control, such as the cyclin-dependent kinases (CDKs),
185 mitogen-activated protein kinases (MAP kinases) and CDK-like kinases (CDKLs). This high degree of
186 conservation is unsurprising given the crucial role these kinases play in fundamental cell biology,
187 especially in proliferating cells. This may provide opportunities for the development of flukicides that
188 disrupt growth via CDK and MAP kinase inhibition. Indeed, inhibitors targeting these kinases have
189 already been developed for cancer treatment [53], and repurposing/redeveloping them to target the
190 neoblast-like cells of *F. hepatica* and other parasitic flatworms could lead to their use as novel
191 anthelmintics.

192 We examined the phylogeny of *F. hepatica* ePKs using CLANs software and found the 'Other' grouping
193 to be the most divergent (Fig 1A). This was not surprising given the diversity of this group which includes
194 the polo-like kinases, NimA-related kinases and aurora kinases among others. In contrast to this, the
195 CMGC family are the most closely clustered, a reflection of their conserved roles. The AGC, CAMK,
196 CK1 and TK families clustered closely with only a few divergent members. However, clustering was
197 more diffuse for the tyrosine-like kinases (TKLs) (Fig 1A), with a bone-morphogenic protein kinase
198 (FhHiC23_g1262) and an integrin-linked protein kinase (FhHiC23_g8606) notable outliers. These
199 divergent sequences may be druggable targets, especially with only a 19-22% sequence identity when
200 compared to their human orthologues. Recent publications in *F. hepatica* have also demonstrated the
201 potential of targeting kinases (protein kinase C β and p21-activated kinase 4) to disrupt motility/viability
202 [27,54].

203 We also identified 17 putative *F. hepatica* aPKs (S2 Table), functional PKs with a typical catalytic kinase
204 fold that lack sequence similarity to ePKs [55]. As in other organisms, there are considerably fewer
205 aPKs than ePKs, though the number identified here is comparable to that found in *C. elegans* [56].
206 Several conserved *F. hepatica* aPKs (S1C Fig) play vital roles in cell proliferation, linking them to their
207 neoblast-like stem cells, such as mammalian target of rapamycin (mTOR), ataxia–telangiectasia
208 mutated kinase (ATM), ataxia–telangiectasia and Rad3 related kinase (ATR) and the phosphoinositide
209 3-kinases [57–59], again highlighting numerous pathways that could be exploited for juvenile fluke
210 control.

211

212 FhPLK expression linked to developing juveniles

213 We used published life-stage transcriptomic data [47] to examine expression profiles of putative PKs.
214 Of the 266 kinases for which we have life stage transcriptomic data, 116 show the highest relative
215 expression in NEJs or immature worms (migrating three-week-juveniles) (Fig 1B). Seven of these genes
216 with enriched expression are *cdk*s, crucial cell cycle regulators [60]. Among them is a putative *cdk1*
217 gene (FhHiC23_g16347) which has been implicated in regulating the pluripotency of embryonic stem
218 cells [61], and can drive the cell cycle in early embryonic cells lacking all other CDKs [62]. Additionally,
219 four putative *F. hepatica* fibroblast growth-factor receptors (*fgfrs*) and two *plks* are most highly
220 expressed in these developing life stages. We also utilised a published transcriptomic dataset that
221 compared *in vitro F. hepatica* juveniles with faster-growing *in vivo* juveniles [46] and found 81% of
222 kinases were more highly expressed in the faster-growing *in vivo* juveniles (Fig 1B), again supporting
223 the hypothesis that kinases play an integral role in growth/development.

224 Development-associated kinases were further interrogated using the *F. hepatica in vitro*/*in* vivo
225 transcriptomic datasets [46] alongside a dataset which identified genes associated with *F. hepatica*
226 neoblast-like cells [21]. Six kinases were downregulated following neoblast-like stem cell ablation, and
227 21 kinases were upregulated in faster-growing worms (S2 Table). Notably, two genes were prominent
228 in both of these datasets, a *fgfr* (FhHiC23_g5821) and *plk1* (FhHiC23_g6132). FGFRs are tyrosine-
229 kinase receptors linked to proliferation [63] with drug inhibition, RNAi or CRISPR-interference in *S.*
230 *mansoni* and *E. multilocularis* reducing neoblast-like cell proliferation [11,12,64,65]. Three FGFR

231 inhibitors have been approved by the FDA for treatment of cancers and idiopathic pulmonary fibrosis
232 [66], highlighting the druggability of these kinases.

233 PLK1 is a core cell cycle effector, regulating centrosome assembly, mitotic entry, the spindle, cytokinesis
234 and more besides [39]. PLK1 has been linked to cell differentiation and survival in other parasitic
235 flatworms [40–43], while in *F. hepatica* its downregulation following irradiation and upregulation in faster
236 growing worms (S2 Table) support its link with neoblast-like stem cells. Our HMM screen and additional
237 BLAST searches identified two further putative *F. hepatica* PLKs (FhPLK2 [FhHiC23_g13468] and
238 FhPLK4 [FhHiC23_g6087]; Fig 2A). However, only FhPLK1 was predicted (full sequence confirmed
239 using transcriptomic reads) to possess all signature PLK1 domains (Fig 2C), including the ATP-binding
240 domain [67], catalytic domains, Mg^{2+} chelating domain [68], phosphorylation site [69] and
241 phosphopeptide binding sites [70,71]. Published life stage transcriptomic data [47] show that *fhplk1*
242 expression peaks in eggs (Fig 2B), potentially indicating significant proliferative cell activity as the
243 embryo develops into the unhatched miracidia, like that seen in *S. mansoni* [72]. Following eggs, relative
244 expression was highest in immature worms and adults, life stages with significant neoblast-like stem
245 cell and germ cell activities respectively [46,73,74]. Moreover, transcriptomic data from Robb et al. (Fig
246 2B, [46]) show greater *fhplk1* and *fhplk4* expression in faster-growing *in vivo* worms, correlating with
247 observed increased cell proliferation. Houhou et al. [44] also found higher *fhplk1* expression in immature
248 worms and adults compared to NEJs (24 h post-excystment) via PCR, though they also observed ~6-
249 fold increase in expression in adults compared to immature worms. The difference seen here between
250 transcriptomic and qPCR methodologies could be due to low replicate numbers in the published
251 transcriptomic datasets [47]. As *plk1* has previously been localised to *S. mansoni* reproductive
252 structures [40], the increased expression in adult *F. hepatica* is likely associated with germ cell activity
253 in this life stage. Together, these transcriptomic data indicate that *fhplk1* is associated with cell
254 proliferation in *F. hepatica*.

255

256 **Fig 2. *F. hepatica* polo-like kinase 1 (PLK1) possesses all functional kinase domains.**

257 (A) Schematic of *F. hepatica* PLKs, with domains as predicted by Interpro, illustrating N-terminal
258 serine/threonine kinase domains and C-terminal polo-boxes. (B) Expression of *fhplk* genes from
259 published datasets; Log_2-transformed median transcripts per mapped million reads (TPMs) of *F.*

260 *hepatica plk* genes across various life stages (egg, metacercariae, 1h NEJ, 3h NEJ, 24h NEJ, 3-week
261 juvenile, adult; [47]); Log_2-transformed median transcripts per mapped million reads (TPMs) of *F.*
262 *hepatica plk* genes in *in vitro and in vivo* 3-week juveniles [46]. (C) Conservation of functional motifs in
263 FhPLK1 but not FhPLK2/4 when compared to PLK1 sequences from *Echinococcus multilocularis*,
264 *Schistosoma mansoni*, *Drosophila melanogaster*, *Homo sapiens* and *Mus musculus*; * = conserved
265 residue, : = highly conserved amino acid properties, . = weakly conserved amino acid properties (our
266 transcriptomic reads were used to confirm sequence).

267

268 RNAi-mediated gene silencing of *fhplk1* disrupts juvenile 269 growth

270 To test if *fhplk1* is integral to maintenance of the *F. hepatica* neoblast-like cell population we employed
271 RNAi to probe its function *in vitro*. Parasites were treated with *fhplk1*-specific dsRNA and monitored for
272 signs of abnormal growth. Transcript knockdown of *fhplk1* was measured after four weeks and found to
273 be reduced by ~90% relative to control treatment (Fig 3A; mean transcript expression ±SEM: control
274 dsRNA = 127.67±9.49%, *fhplk1* dsRNA = 9.33±2.73%). We also found that transcript expression of
275 another proliferative cell marker (histone 2b (*fhh2b*)) was reduced by 81.7±9%. Though not significantly
276 different, it suggested that *fhh2b* expressing cells were depleted in *fhplk1*-RNAi worms; expression of
277 a muscle cell marker (myosin light-chain (*fhmlc*)) was reduced by 21.3±30% relative to untreated
278 worms, although again this was not significant (Fig 3A). H2B is highly expressed throughout the S-
279 phase of the cell cycle when it participates in chromatin organisation [75]. Histone depletion reduces
280 cell-cycle progression [76,77] and RNAi-mediated silencing in free-living and parasitic flatworms impairs
281 proliferation, leading to a failure in tissue regeneration/maintenance [12,16,21,78]. Here, we observed
282 that *fhplk1*-RNAi affected fluke development *in vitro*, with *fhplk1*-RNAi juveniles significantly smaller
283 than control worms three weeks after the first RNAi trigger (Fig 3B; mean juvenile area ±SEM at three-
284 weeks: untreated = 97350±2559 μm^2, control-dsRNA = 94214±4266 μm^2, *fhplk1* dsRNA = 73964±2559
285 μm^2). This phenotype was further exaggerated after a fourth week (Fig 3B; mean juvenile area ±SEM
286 at four-weeks: untreated = 118368±4732 μm^2, control-dsRNA = 117781±5130 μm^2, *fhplk1* dsRNA =
287 75942±2495 μm^2). We also found that *fhplk1* knockdown impaired cell proliferation in four-week-old

288 juveniles, thereby disrupting the neoblast-like stem cell population (Fig 3C & D; mean # EdU$^+$ nuclei
289 ±SEM: control-dsRNA = 477.5±47; *fhplk1*-dsRNA = 9.8±5.4). RNAi of *plk1* in mammalian cancer cell
290 lines *in vitro* also reduced proliferation [79], and reduced tumour size *in vivo* in mice with non-small cell
291 lung carcinoma [80], supporting a conserved role for *plk1* in proliferative cells. Interestingly, following
292 four weeks of *plk1* silencing, juveniles cultured for a week in the absence of a RNAi-trigger showed no
293 signs of recovery and did not resume proliferation (S2 Fig); this observation is consistent with the
294 hypothesis that prolonged *fhplk1*-RNAi results in the ablation of *F. hepatica* neoblast-like stem cells.
295 Together, these data support a conserved function for PLK1 in *F. hepatica* that ensures cell-cycle
296 progression. As PLK1s are functionally conserved in *S. mansoni* and *E. multilocularis* [40,43], targeting
297 PLK1 activity could be an effective pan-phylum control strategy.

298

299 **Fig 3. Knockdown of *fhplk1* disrupts growth and cell proliferation in juvenile *Fasciola hepatica***
300 ***in vitro*.**
301 (A) Mean expression ±SEM of *fhplk1* (white), *fhh2b* (green) and *fhmlc* (purple) relative to *fhgapdh* in
302 juvenile *F. hepatica* following four weeks of repeated exposures to *fhplk1* dsRNA *in vitro* shows
303 significant knockdown of *fhplk1* and reduction in expression of neoblast-like cell associated gene *fhh2b*
304 relative to control dsRNA treated worms (unpaired t tests). (B) Mean area ±SEM of juvenile *F. hepatica*
305 significantly diminished over three/four weeks of *fhplk1* dsRNA exposures (Kruskal-Wallis and Dunn's
306 posthoc tests). (C) Mean # EdU$^+$ nuclei ±SEM significantly decreased after four weeks of *fhplk1* dsRNA
307 treatments in juvenile *F. hepatica* (Mann-Whitney U test). (D) Confocal images of EdU staining (green)
308 in four-week-old *F. hepatica* treated with *fhplk1* dsRNA *in vitro* shows reduction in # EdU$^+$ nuclei
309 compared to control dsRNA treated worms; scale bar = 100 μm, DAPI counterstain (magenta). **,
310 $p<0.01$; ***, $p<0.001$; ****, $p<0.0001$.

311

312 RNAi of *fhplk1* downregulates cell cycle effectors and
313 ribosome biogenesis

314 We previously used irradiation to identify transcripts associated with *F. hepatica* neoblast-like cells [21].
315 However, while irradiation is effective at ablating proliferating cells, the potential for damage to
316 differentiated cells limits its utility. Transcriptomic analysis following *fhplk1* silencing would help inform
317 *fhplk1*'s role in juvenile fluke and support identification of other genes associated with
318 growth/development. Therefore, we carried out target-specific RNAi for three weeks before worm
319 extraction and transcriptome sequencing (Fig 4A), confirming that *fhplk1*-RNAi reduces growth and
320 ablates neoblast-like stem cells (S3A & B Fig). RNA-Seq was then used to identify differentially
321 expressed genes (DESeq2, padj < 0.001; S4 Table), with 946 downregulated genes and 1244
322 upregulated genes (Fig 4B). TOPGO analysis showed that genes associated with protein translation,
323 ribosome assembly and DNA replication were overrepresented among downregulated genes (Fig 4C).
324 The downregulation of genes associated with protein synthesis ('translation' and 'protein folding'; Fig
325 4C) was interesting as studies in mouse cells showed that protein synthesis rates in early differentiated
326 mouse cells are two-fold of that in embryonic stem cells [81], a result also observed in other mammalian
327 cell cultures (reviewed in [82]). As *fhplk1*-RNAi depletes neoblast-like cells (i.e. stem cells) the
328 proportion of differentiated cells might be expected to increase relative to control worms, although the
329 production of more undifferentiated cells in the control groups could explain the higher levels of protein
330 synthesis. Further, other GO terms ('ribosomal small subunit assembly', 'structural component of
331 ribosome'; Fig 4C & S3C Fig) suggested that the downregulation of translation may be related to
332 reductions in ribosomal activity. KEGG pathway analysis showed the downregulation of ribosomal
333 subunits/biogenesis following *fhplk1*-RNAi (S3D Fig) which matches observations in other platforms
334 where stem cells have lower translation rates than differentiated cells, except in the case of ribosome
335 biogenesis, which is upregulated in proliferating cells [83]. The downregulation of ribosome biogenesis-
336 associated genes was also observed 14 days after irradiation in *S. mansoni* [13], demonstrating that
337 this occurs in related species. It is also possible that the differential expression of ribosome-associated
338 genes/pathways is indicative of general stress, as downregulation of these genes/pathways has
339 previously been noted in nematodes following drug treatment (with non-stem cell targeting drugs) and
340 local environment change [84,85].

341

342 **Fig 4. *fhplk1* knockdown downregulates cell cycle and translation-associated transcripts in**
343 **juvenile *Fasciola hepatica in vitro*.**

344 (A) Experimental timeline showing dsRNA treatments (24 h dsRNA exposure each time) carried out on
345 juvenile *F. hepatica* across three weeks to generate transcriptomes with final treatment from day 21-22.
346 (B) Volcano plot showing differentially expressed genes (red dots; DESeq2, padj < 0.001) after *fhplk1*
347 RNAi in juvenile *F. hepatica* where blue shading indicates downregulated genes and red shading
348 indicates upregulated genes. (C) Top 10 overrepresented biological process GO terms among
349 downregulated genes following *fhplk1* RNAi shows genes involved in translation and nucleotide
350 interactions. (D) Many components of KEGG cell cycle pathway downregulated following *fhplk1* RNAi
351 (red = upregulated; grey = no change; blue = downregulated; white = unassigned KEGG ID). (E) Venn
352 diagram showing overlap between genes downregulated following *fhplk1* RNAi in juvenile *F. hepatica*,
353 irradiation in juvenile *F. hepatica* (green) or irradiation in adult *S. mansoni* (yellow). (F) Log_2foldchange
354 of differentially expressed kinases following *fhplk1* RNAi shows downregulation of proliferation-
355 associated kinases such as MAPKs and FGFRs (colours correspond to log_2foldchange; red =
356 upregulated; blue = downregulated).

357

358 Transcripts associated with DNA/RNA interactions and the cell cycle were also downregulated following
359 *fhplk1* knockdown (e.g. DNA-replication initiation; Fig 4C & S3 Fig). Indeed, 4/5 KEGG pathways
360 downregulated following irradiation of *F. hepatica* juveniles [21] were downregulated following *fhplk1*
361 RNAi (S3D Fig). The absence of actively proliferating cells following *fhplk1*-RNAi, and concurrent
362 downregulation of cell cycle-associated transcripts adds to the evidence that proliferative cells in the
363 somatic tissue of juvenile/immature fluke are analogous to the neoblast-like stem cells of other parasitic
364 flatworms [12,13,16]. Numerous core cell cycle genes were downregulated (S3 Table), including *atm*
365 and *atr* kinases, *p53*, cell division control proteins, *cyclinB*, members of the mini-chromosone complex
366 (*mcm2-7*) and origin recognition complex subunits (*orc2 & 3*). Additional core cell cycle regulators not
367 annotated by eggNOG, but identified through BLAST searches, were also downregulated, such as a
368 p53 homologue (FhHiC23_g6525). p53 is a tumour suppressor which can arrest the cell cycle and
369 cause apoptosis when activated [86]. Mutations in p53 are linked to cancerous growths, with
370 compounds developed to reverse these adverse mutation effects currently in clinical trials [87].
371 Furthermore, a *S. mansoni* p53 homologue has been linked to their neoblast-like cells [18]. While many
372 of the cell cycle effectors discussed likely have conserved structure/function in both parasites and their

373 hosts, inhibitors that indirectly target them [88] may be worth exploring for their anthelmintic potential.
374 One surprising observation in the cell cycle schematic was 'upregulation' of *fhplk1* following *fhplk1* RNAi
375 (DESeq2, *fhplk1* $\log_2$Fold Change = ↑ 3.73). Our earlier trials had confirmed *fhplk1* knockdown following
376 dsRNA treatment via qPCR (Fig 3A) so this upregulation was unexpected. However, examination of the
377 read files via the Integrative Genomics Viewer (https://igv.org/) revealed that *fhplk1* dsRNA was likely
378 sequenced as reads were observed only in the 192 bp dsRNA amplicon region of *fhplk1* dsRNA samples
379 (S3E & F Fig). Control dsRNA samples on the other hand had reads across the length of the gene, with
380 exons clearly visible (S3E Fig). The data indicate that this sequencing anomaly is related to our RNAi
381 methodology as we ensure knockdown by repeatedly soaking worms in 100 ng/µL dsRNA) [89],
382 including the 24 h period immediately preceding worm extraction.

383 We aimed to identify pan-trematode transcripts clearly linked to parasitic flatworm neoblast-like cells by
384 cross-referencing the transcriptomic data generated here against the transcriptomes of irradiated *S.*
385 *mansoni* and *F. hepatica* [12,21]. We found 21 genes downregulated in all three transcriptomic datasets
386 following neoblast-like cell ablation (Fig 4E; note that the relatively small number of downregulated
387 genes found in both irradiated datasets is likely due to the different life stages investigated as discussed
388 in [21]). Many of the genes downregulated in all three datasets are known for their links to proliferation
389 (S4 Table), including the cell cycle regulators *p53*, *cyclinB* and the *mcm* complex members. A further
390 34 genes were downregulated following *fhplk1*-RNAi in *F. hepatica* and irradiation in *S. mansoni*,
391 including *hepatic leukaemia factor*, *mastL* (*greatwall kinase*) and *wdhd1* (*WD repeat and HMG-box*
392 *DNA-binding protein/and-1*) which again have been associated with cell cycle regulation [90], DNA
393 replication [91] and stem cell population maintenance [92]. Finally, 46 genes were downregulated in *F.*
394 *hepatica* following either *fhplk1*-RNAi or irradiation with eight transcription factors/regulators included
395 among them as well as an *fgfr*, implying conserved roles related to *F. hepatica* neoblast-like cells. While
396 there were these shared downregulated genes between these two *F. hepatica* datasets there were 879
397 genes only downregulated following *fhplk1*-RNAi (Fig 4E). We hypothesise that this difference is caused
398 by the loss of neoblast-like cells over an extended 3-week period of time (unlike the irradiated dataset
399 in which juveniles were sequenced 48 hours after X-ray exposure), with this having knock-on effects
400 across tissues in the worm.

401 As several of the genes downregulated in both datasets were kinases we explored the expression all
402 *F. hepatica* kinases following *fhplk1* RNAi; 48 kinases were differentially expressed (22 downregulated

403 and 26 upregulated; Fig4 F). Among downregulated kinases were three *fgfrs* that were also upregulated
404 in developing life stages (FhHiC23_g6174, FhHiC23_g1614 and FhHiC23_g5821), an aurora kinase
405 and members of the MAPK signalling cascade which regulates cell cycle progression [93]. Again, these
406 kinases are integral to activate proliferation in other species and may be appealing targets for control.
407 AGC kinases and CAMKs were more represented among upregulated kinases, though their functions
408 are more diverse and less clearly linked to proliferation.

409 One final point to note is that of 46 genes downregulated after irradiation or *fhplk1*-RNAi in *F. hepatica*,
410 ten had no clear BLAST hit in model species, though they all have *S. mansoni* homologues and most
411 have *F. gigantica* homologues. Furthermore, of the 50 most downregulated transcripts (ranked by fold-
412 change) only 8 had clear BLAST hits in model species (e-value <0.001, S3 Table), though most were
413 found to have orthologues in at least one other parasitic flatworm. While we know little of the function
414 of these genes/proteins, their downregulation links them to putative roles in *F. hepatica*
415 growth/development associated with neoblast-like stem cells, especially where also downregulated
416 following irradiation. These unknown genes could be attractive drug targets, given their lack of
417 homology to genes in host species.

418

419 Inter-cell signalling upregulated following *fhplk1* RNAi

420 Over 1200 juvenile fluke genes were upregulated following three weeks of *fhplk1*-RNAi (Fig 4B; S3
421 Table). TOPGO analysis of these genes showed that GO terms associated with inter-cell signalling
422 systems such as ion transport, cell-adhesion and synapses were overrepresented (Fig 5A; S4A Fig)
423 among the upregulated genes. Furthermore, cellular component GO terms suggested many predicted
424 proteins are associated with the cell membrane and extracellular space/synapse (S4A Fig), supporting
425 evidence for the upregulation of inter-cell signalling. KEGG pathway analysis further reinforced this,
426 highlighting upregulation of multiple neuronal-ligand receptors, including many GPCRs (Fig 5B). Many
427 signalling pathways were also upregulated, such as those linked to the gap junction as well as
428 GABAergic, serotonergic and cholinergic synapses (S4B Fig). Gap junctions are critical to cell-cell
429 connectivities that help coordinate cellular functions in multicellular organisms, though invertebrates
430 lack the associated connexin proteins and instead possess innexins [94]. While the gap junction itself

431 is unmarked in the KEGG pathway of S4C Fig as the pathway is based on that of humans, we found
432 five predicted innexins to be significantly upregulated following *fhplk1*-RNAi (FhHiC23_g648,
433 FhHiC23_g6222, FhHiC23_g9940, FhHiC23_g15433 and FhHiC23_g15004; S3 Table). Innexins have
434 been localised in various planarian tissues, including the nervous system [95], and their inhibition can
435 lead to developmental abnormalities through polarity disruption during regeneration [95,96], or ablation
436 of neoblast-cell populations [97], suggesting key roles in developmental regulation.

437

438 **Fig 5. RNAi of *fhplk1* in *Fasciola hepatica* results in upregulation of inter-cell signalling systems.**
439 (A) Biological process GO terms (top 10) associated with ion transport and cell signalling are
440 overrepresented among upregulated genes following *fhplk1* RNAi. (B) KEGG pathway showing
441 upregulation of several neuroactive-ligand receptors following *fhplk1* RNAi (red = upregulated; grey =
442 no change; blue = downregulated; white = unassigned KEGG ID; red box = unassigned KEGG ID but
443 identified as upregulated from BLAST searches). (C) Log_2foldchange ±SEM of putative *F. hepatica*
444 neuropeptides following *fhplk1* RNAi shows all 22 upregulated, with 15 differentially expressed (black
445 bars). (D) Log_2foldchange of differentially expressed putative receptors and channel subunits (identified
446 via BLAST searches) following *fhplk1* RNAi shows upregulation of 134/155 (colours correspond to
447 log_2foldchange; red = upregulated; blue = downregulated).

448

449 Within the upregulated classical transmitter pathways there was upregulation of ligand synthesis
450 enyzmes, receptors and downstream signalling molecules such as G proteins (GABAergic example
451 shown in S4D Fig). Indeed, of the known *F. hepatica* classical transmitter pathways [98], only the
452 histamine pathway had no evidence (based on TOPGO, KEGG and BLAST analysis) of upregulation,
453 a poorly understood pathway in parasitic flatworms [99]. Curiously, some upregulated classical
454 transmitter pathways have opposing effects on *F. hepatica* motility (e.g. acetylcholine is believed to be
455 inhibitory [100], while serotonin is excitatory [101]), making their concurrent upregulation interesting and
456 potentially linked to increased tonic regulation. Serotonin has been implicated in proliferation in other
457 species [102–105] and has been shown to directly stimulate growth/proliferation in *S. mansoni* and *E.*
458 *multilocularis* [106,107]. While the roles of acetylcholine and dopamine in flatworm growth are unknown,
459 they have been linked to proliferation in mammals [108,109]. Furthermore, dopamine deficiency in *C.*

460 *elegans* and *D. melanogaster* constrains development [110,111] and a dopamine antagonist reduced
461 *S. mansoni* miracidial transformation [112]. *C. elegans* lacking choline acetyltransferase (ChAT) also
462 display slower growth [113].

463 Additionally, 16/22 putative neuropeptide encoding genes identified in our dataset (S5 Table) were
464 significantly upregulated in *plk1*-RNAi worms (Fig 5C), as were their processing enzymes; *prohormone*
465 *convertase 2* (*pc2*; FhHiC23_g9059), *carboxypeptidase E* (*cpe*; FhHiC23_g10997), *peptidylglycine*
466 *alpha-hydroxylating monooxygenase* (*phm*; FhHiC23_g3039) and *peptidyl-alpha-hydroxyglycine alpha-*
467 *amidating lyase* (*pal*; FhHiC23_g9107), along with several predicted neuropeptide receptors (Fig 5B).
468 Neuropeptides have been shown to drive mammalian cell proliferation [114], as well as germline
469 proliferation and regeneration in planarians [115–118]. Furthermore, two neuropeptides and their
470 GPCRs are required for normal maturation of female reproductive structures in *S. mansoni* [119]. If
471 classical transmitters and neuropeptides have conserved roles in managing growth/proliferation in *F.*
472 *hepatica,* then the upregulation observed could indicate that *fhplk1*-RNAi juveniles lacking neoblast-like
473 cells are attempting to boost cell proliferation via enhancement of selected inter-cell signalling systems.

474 Previously, we highlighted that signalling systems were upregulated in slower growing *F. hepatica* with
475 decreased cell proliferation [46]. Here we saw the loss of neoblast-like stem cells, concomitant with
476 nervous system upregulation, indicating potential interplay between proliferating neoblast-like stem
477 cells and neuronal signalling systems. When we compared upregulated genes in our neoblast-like stem
478 cell ablated juveniles with downregulated genes in neoblast-like stem cell-enriched *in vivo* juveniles
479 [46], we identified 244 shared genes, including 12 neuropeptide encoding-genes (S6 Table). Further,
480 TOPGO analysis of these genes showed that neurotransmitter and Wnt signalling were enriched (S4E
481 Fig). Enrichment of the Wnt pathway is notable as Wnts support proliferation and polarity orientation in
482 regenerating planarians [120], with similar roles proposed in parasitic flatworms [121–123]. RNAi of *wnt*
483 genes in regenerating planarians can result in aberrant neurogenesis [124–127] and their silencing was
484 recently shown to inhibit *F. hepatica* neoblast-like cell proliferation and growth/development *in vitro*
485 [128].

486 To help us understand the scale of signalling upregulation we examined all BLAST results for the terms
487 'receptor' or 'channel' to identify putative intercellular signalling-related genes. Of the 155 putative
488 receptors/channels identified through BLAST searches, 134 (86%) were significantly upregulated

489 following *plk1*-RNAi (Fig 5D). Those that were downregulated were mainly kinases or nucleus-
490 associated transporters that could be associated with worm neoblast-like stem cells. S4G Fig shows
491 that 22% of the upregulated receptors/channels were predicted rhodopsin peptide GPCRs with voltage-
492 gated potassium channel subunits constituting another large component. Among these genes were two
493 putative FMRFamide-activated amiloride-sensitive Na+ channel subunits [129] that may be of interest
494 as putative drug targets due to their unusual pharmacology and proposed absence in mammals. These
495 data illustrate the extent of upregulation seen within signalling systems following sustained *fhplk1*-RNAi.

496 We recognise that the reduced size of *plk1*-dsRNA worms (in comparison to control dsRNA worms)
497 may increase the proportionality of neuronal tissue, thereby increasing the balance of neuronal-
498 associated transcripts. However, tissue proportionality does not appear to be a key factor in the
499 observed upregulation for a variety of reasons. Firstly, while *fhplk1*-RNAi worms were indeed smaller
500 (S3A Fig), the difference in size was modest compared to that seen in the gene-function RNAi trials (Fig
501 3B). Furthermore, while we found DAPI staining (calculated as a percentage of worm area) decreased
502 following *fhplk1*-RNAi (S4F Fig), the decrease was ~20% which may be directly attributable to the
503 absence of neoblast-like stem cells (neoblasts account for around 20-35% of all cells in free-living
504 flatworms [130]). Second, another study observed the downregulation of signalling systems in faster
505 growing, stem cell enriched *F. hepatica* [46], with much greater size differences (~15x) than those
506 observed in our study. Despite this, genes associated with signalling had comparable fold changes in
507 expression in most instances (S7 Table), again suggesting size/tissue proportionality is not a factor in
508 nervous system upregulation. Thirdly, we did not observe consistent upregulation of transcripts
509 associated with other tissue types, such as the tegument (*tsp2*) or the gut (18 cathepsins upregulated
510 and 14 downregulated) which indicates that the nervous system transcript upregulation is unusual.
511 Finally, we found this pattern of increased signalling in adult male *S. mansoni* datasets in which worms
512 were subjected to transcriptomics two weeks after irradiation, or three weeks after the onset of *smfgfrA*
513 or *smh2b* RNAi [13]. TOPGO analysis of these datasets showed again that there was an increase in
514 transcripts associated with signalling systems, ion transport and cell communication (S8 Table). Given
515 that these worms were adults of comparable size and that the anterior portion, including cerebral
516 ganglia, had been removed (to exclude testes from analysis) the upregulation of signalling systems
517 following neoblast-like stem cell ablation in diverse circumstances supports the validity of these
518 transcriptional changes in neuronal signalling systems and warrants further investigation.

519 These data challenge the traditional orthodoxy of using short-term motility-based assays to assess the
520 drug target candidature of various helminth signalling pathways. If the signalling systems highlighted in
521 this study do play significant roles in cell proliferation, then potential long-term impacts of drugs on worm
522 growth/development could be missed with restricted phenotype monitoring windows. Glutamate-gated
523 chloride channels and nicotinic acetylcholine receptors are already targets of current anthelmintics,
524 while GPCRs are thought of as highly 'druggable' targets [131]. Repurposing drugs to disrupt neoblast-
525 like stem cell biology could expose novel control strategies.

526

527 No correlation between DE miRNAs and predicted DE mRNA 528 targets

529 We carried out miRNA sequencing on the same RNA samples and used miRDeep2 to map reads to the
530 150 predicted miRNAs [132]. We found 68 of these miRNAs were expressed in at least two of the six
531 samples, with 13 downregulated and 8 upregulated (S5A Fig; DESeq2, padj <0.001; S9 Table). Target
532 prediction software was then used to identify putative target transcripts of these differentially expressed
533 miRNAs (S9 Table). TOPGO analysis did not identify any enriched GO terms among potential target
534 transcripts. We then plotted GO term frequency of predicted target transcripts against fold change (S5B
535 Fig) but found little, to no overlap with GO terms of differentially expressed mRNAs. Finally, only 36
536 targets predicted to be downregulated were found to be so, while only 38 of those predicted to be
537 upregulated were so. No clear links between *fhplk1*-RNAi silencing in juvenile *F. hepatica* and
538 endogenous miRNA activity were uncovered.

539

540 Pharmacological inhibition of FhPLK1 phenocopies *fhplk1*- 541 RNAi

542 We next assessed the drug-target candidature of FhPLK1 through use of the commercially available
543 inhibitor BI 2536. Overexpression of PLK1 in various cancers has led to the development of inhibitors,

544 including BI 2536, a highly selective PLK1 inhibitor which can blunt cell proliferation in various cancer
545 types, both *in vitro* and *in vivo* [133,134]. As BI 2536 is an ATP-competitive inhibitor [133], high levels
546 of sequence similarity across human PLK1-3 kinases compromises its selectivity [133,134]. As
547 discussed previously we identified two additional PLK genes in *F. hepatica*, one similar to human PLK2
548 (FhPLK2), with the other similar to both human PLK4 (FhPLK4) and SAK (Serum-inducible kinase Akin
549 Kinase) in *S. mansoni* and *E. multilocularis* [43,135]. PLK4 divergence in humans renders it less
550 sensitive to BI 2536 [133], a trait also observed for *S. mansoni* SmSAK [135]. Crystallisation
551 experiments identified Leu_{132} of HsPLK1 as a key residue for facilitating drug-target interaction and
552 selectivity. This leucine was conserved in FhPLK1 (Leu_{104}), but not in FhPLK2 or FhPLK4 (S6A Fig),
553 suggesting that the activity of BI 2536 would be specific to FhPLK1 in *F. hepatica*.

554 Initial experiments involved exposing NEJs to a broad range of BI 2536 concentrations (0.001 μM – 10
555 μM) for 18 hours in RPMI, with motility measured as an indicator of viability as motility of *F. hepatica*
556 had previously been disrupted following BI 2536 exposure [45]. However, in our hands, none of the BI
557 2536-treated groups exhibited reduced motility (S6B Fig). We monitored rhythmic movement (length of
558 individual parasites plotted across frames) for subtle motility changes (S6C Fig), finding that even those
559 treated with 10 μM BI 2536 retained the classical, 'accordion'-style movement associated with *F.*
560 *hepatica* NEJs (rhythmical lengthening and shortening in a probing fashion) [136]. This was in stark
561 contrast to treatment with 1 μM TCBZ which paralysed juveniles (S6C Fig). Our BI 2536 results are not
562 directly comparable to those of Morawietz et al. [45] as they treated older worms (*ex vivo* immature and
563 adults) with higher concentrations (20 μM – 100 μM).

564 As neoblast-like cell inhibition is associated with growth defects [20,21], worms were treated with BI
565 2536 for 18 h and then cultured for one week in the absence of drug. There were no significant
566 differences between the sizes of juveniles from any treated group and the DMSO-treated controls (Fig
567 6A). However, incubation of a subset of juveniles with EdU showed significantly reduced proliferation in
568 those treated with 10 μM BI 2536 (Fig 6B; # EdU^+ nuclei ±SEM: DMSO = 465.1±109.5, 10 μM BI 2536
569 = 55.1±25.9). A small reduction in EdU^+ nuclei was also seen in juveniles treated with 1 μM BI 2536,
570 though this difference was not significant. These data suggest that culture following drug exposure
571 afforded the opportunity for fluke to recover. To test this, parasites were cultured for one week before
572 treatment with BI 2536 and subsequent EdU exposure. These worms displayed concentration-
573 dependent reduced cell proliferation across all groups, with significance observed at both 1 μM and 10

574 μM BI 2536 (Fig 6C; # EdU⁺ nuclei ±SEM: DMSO = 173.8±11.5, 1 μM BI 2536 = 12.7±4.7, 10 μM BI
575 2536 = 0±0). The observed phenotypic responses are consistent with BI 2536 inhibiting PLK1 activity
576 in *F. hepatica*, matching observations in other parasitic flatworms [40,43].

577

578 **Fig 6. Repeated exposure of juvenile *Fasciola hepatica* to the PLK1 inhibitor BI 2536 *in vitro***
579 **reduces growth and proliferation.**
580 (A) Mean worm area ±SEM of 7-day-old juvenile *F. hepatica* after exposure to BI 2536 on day 0, followed
581 by 7 days in culture, shows no effect on growth. (B) Mean # Edu⁺ nuclei ±SEM in 9-day-old *F. hepatica*
582 after exposure to BI 2536 on day 0, followed by 8 days in culture, shows 10 μM significantly reduced
583 the number of proliferating cells. (C) Mean # Edu⁺ nuclei ±SEM in 9-day-old *F. hepatica* after exposure
584 to BI 2536 on day 7, shows both 1 μM and 10 μM significantly reduced the number of proliferating cells.
585 (D) Mean area (μm^2) ±SEM of *F. hepatica* across 13 days following BI 2536 exposures on days 0, 4
586 and 8 shows 10 μM significantly reduced growth rate. (E) Mean # Edu⁺ nuclei ±SEM in 14-day-old *F.*
587 *hepatica* after repeated BI 2536 exposures on days 0, 4 and 8 (timeline from (E) applies to this graph)
588 shows all tested concentrations significantly reduced the number of proliferating cells. (F) Mean size of
589 Edu⁺ nuclei ±SEM in 14-day-old *F. hepatica* after repeated BI 2536 exposures (1 and 10 μM) on days
590 0, 4 and 8 (timeline from (E) applies to this graph) shows increased nuclei area. (G) Confocal images
591 of EdU staining (green) in 14-day-old *F. hepatica* exposed to various concentrations of BI 2536 on days
592 0, 4 and 8 shows a dose-dependent reduction in # EdU⁺ nuclei and increase in EdU⁺ nuclei area
593 compared to DMSO-treated control; scale bar = 100 μm, DAPI counterstain (magenta). *, $p<0.05$; ***,
594 $p<0.001$; ****, $p<0.0001$.

595

596 As BI 2536 disrupted neoblast-like cell proliferation we investigated whether it could inhibit juvenile
597 development. For these experiments, parasites were treated with BI 2536 multiple times (on days 0, 4
598 and 8) with measurements taken on days 1, 5, 9 and 13. After 9 days, worms treated with 10 μM were
599 significantly smaller than control worms (Fig 6D; day 9 mean juvenile area ±SEM: DMSO = 42368±1286
600 μm^2, 10 μM BI 2536 = 33861±907 μm^2). This phenotype was still evident following a drug-free period
601 post treatment (Fig 6D; day 13 mean juvenile area ±SEM: DMSO = 57568±2035 μm^2, 10 μM BI 2536
602 = 43799±1122 μm^2). EdU exposure revealed significant, concentration-dependent reductions in cell

603 proliferation across all groups (Fig 6E & G; # EdU$^+$ nuclei ±SEM: DMSO = 423.8±72.3, 0.1 μM BI 2536
604 = 268.6±35.5, 1 μM BI 2536 = 107±10, 10 μM BI 2536 = 6±1.8). These results largely phenocopy those
605 seen following *fhplk1*-RNAi (Fig 3), supporting FhPLK1's conserved regulatory role in the proliferation
606 of *F. hepatica* neoblast-like stem cells. We noticed that EdU$^+$ nuclei appeared larger in worms treated
607 with higher concentrations of the drug. Therefore, we measured 10 randomly selected EdU$^+$ nuclei from
608 five juveniles in each treatment group. This revealed that the EdU$^+$ nuclei were significantly larger in
609 worms treated with 1 μM and 10 μM BI 2536 (Fig 6F & G; EdU$^+$ nuclei area: DMSO = 63.2±1.6 μm^2, 1
610 μM BI 2536 = 114.3±8.2 μm^2, 10 μM BI 2536 = 142.1±18.1 μm^2). These larger nuclei could be indicative
611 of neoblast-like cells that had passed through S phase before being delayed/arrested at either the G2/M
612 transition or during mitosis. BI 2536 has previously been shown to increase the DNA content in cancer
613 cells, which was attributed to an inability to undergo cytokinesis [134]. We did not observe larger EdU$^+$
614 nuclei throughout our RNAi experiments. This could be due to the short-term effects of inhibitor
615 exposure which could be reversed following its removal in contrast to the long-term systemic changes
616 to the biology of the worms throughout *fhplk1* RNAi [137].

617 While BI 2536 has previously been shown to affect *F. hepatica* movement *in vitro* [45], our *plk1*-RNAi
618 and pharmacological inhibition experiments highlight how disrupting FhPLK1 activity can undermine
619 neoblast-like cell mediated growth and development. This could weaken *F. hepatica* juveniles within the
620 host environment, aiding parasite clearance by the immune system. BI 2536 has proven anthelmintic
621 activity against both *S. mansoni* and *E. multilocularis*, disrupting gamete production and preventing
622 metacestode formation from germinative cells, respectively [40,43]. Taken together, these data suggest
623 that developing/repurposing drugs to target PLKs could be a promising anthelmintic strategy to control
624 a range of parasitic flatworms, including different life stages.

625

626 # Conclusion

627 This study encourages exploration of parasitic flatworm neoblast-like cells as targets for novel
628 anthelmintics. Our annotation of the *F. hepatica* kinome showed that many kinases linked to proliferation
629 are enriched in the highly pathogenic immature life stages. Functional genomics and inhibitor trials
630 validated this approach as disruption of *fhplk1*, a core cell cycle-related kinase, diminished proliferation

631 in the neoblast-like stem cell population and undermined worm growth/development. This approach
632 could be expanded to other kinase targets such as the additional putative PLKs or the FGFRs. Indeed,
633 the *S. mansoni* SmSAK gene has conserved roles in cell cycle progression [54], and knockdown
634 reduced schistosomula viability *in vitro* [33]. Moreover, the ability of a kinase inhibitor to disrupt *F.*
635 *hepatica* growth/development adds credence to the idea of targeting parasitic flatworm kinases [138],
636 perhaps even in combination with current flukicides, to improve efficacy in cases of reduced drug
637 susceptibility/resistance.

638 Our transcriptomic analyses highlighted possible links between *F. hepatica* neoblast-like cells and
639 neuronal/signalling systems. Neurotransmitter signalling systems have long been touted, and exploited,
640 as anthelmintic targets. However, if novel roles for these systems in parasitic flatworm
641 growth/development are uncovered it opens new paths to target discovery and exploitation for drug
642 development. A significant panel of genes were downregulated following *fhplk1*-RNAi, suggesting they
643 have some role in mitotic regulation/stem cell biology in fluke. The work here has built new
644 understanding of neoblast-like cell directed growth/development in *F. hepatica* which will enhance the
645 opportunities for novel control target discovery.

Methods

Identification of putative *F. hepatica* protein kinases

The PK sequences of the nine *Homo sapiens* ePK families, along with the aPKs, were downloaded from Uniprot (https://ftp.uniprot.org/pub/databases/uniprot/current_release/knowledgebase/complete/docs/pkinfam.txt). HMMER (v3.4; http://hmmer.org/) was used to assemble query sequences for each ePK family and the aPKs. HMM searches were carried out using HMMER against the University of Liverpool and Washington University *F. hepatica* predicted proteomes [47,139] downloaded from Wormbase ParaSite (WBPS18, https://parasite.wormbase.org) [140]. We also looked for additional kinases in a set of novel transcripts. These were generated by aligning all publicly available *F. hepatica* transcriptomic reads [21,46,47] and in-house transcriptomic datasets against the University of Liverpool genome (WBPS19, https://parasite.wormbase.org/Fasciola_hepatica_prjeb58756/Info/Index/) using HISAT2 (v.2.1.0), before transcript assembly with Stringtie (v1.3.6) to create a master reference gtf file containing 14,684 'novel' transcripts that did not overlap with genes in the reference assembly. All putative hits were screened via BLAST searches against the SwissProt database, and domains annotated using InterPro (https://www.ebi.ac.uk/interpro/about/interproscan/). Hits were retained only when the top BLAST result was a PK, and when a kinase domain was predicted to be present. Duplicates/putative gene copies were identified using Clustal Omega (https://www.ebi.ac.uk/Tools/msa/clustalo/) and manually inspected before removal. The remaining putative *F. hepatica* PKs were used to create two HMM query sequences (one ePK and one aPK) which were then used in further HMM searches against both *F. hepatica* predicted proteomes [47,139] to ensure no PKs were missed. Resulting hits were sorted through the same pipeline. BLAST results were used to classify which family/subfamily putative *F. hepatica* kinases belonged to.

Putative ePKs were clustered using CLANs analysis software (1,000,000 rounds of clustering; [141]). MEGA11 (https://megasoftware.net/, [142]) was used to align aPKs (ClustalW), identify the optimum model for phylogenetic analysis, and construct a Maximum Likelihood (ML) tree with 500 bootstraps. This ML tree was visualised using the Interactive Tree of Life (https://itol.embl.de/).

673 Published life-stage transcriptomic data from eggs, metacercariae, 1 h newly excysted juveniles (NEJs),
674 3 h NEJs, 24 h NEJs, three-week juveniles and adults [47] were used to obtain median TPM values for
675 all predicted PKs. Z scores were generated, and heatmaps produced using Morpheus software
676 (https://software.broadinstitute.org/morpheus).

677

678 *F. hepatica in vitro* excystment and culture

679 The Italian strain of *F. hepatica* (Ridgeway Research, UK) was used for all experiments. Excystments
680 were carried out as previously described [89,143], and a detailed protocol is available at
681 https://dx.doi.org/10.17504/protocols.io.14egn212qg5d/v1. Briefly, metacercariae were physically
682 'popped' from their outer cyst walls and treated with 10% (v/v) sodium hypochlorite (#1056142500,
683 Sigma-Aldrich) diluted in double-distilled water (ddH_2O) for 2-3 minutes (exact time dependent on
684 metacercariae batch). Popped and bleached metacercariae were then washed in ddH_2O at least five
685 times to remove excess sodium hypochlorite, prior to being stimulated to excyst as detailed by McVeigh
686 et al. [143]. Parasites were cultured in 200 µL CS50 (50% (v/v) chicken serum (#16110082, Thermo
687 Fisher Scientific) in RPMI (#11835105, Thermo Fisher Scientific) with antibiotic/antimycotic (#A5955,
688 Sigma Aldrich)) in 96-well, round-bottomed plates (#83.3925, Sarstedt) in a humidified incubator at 37°C
689 with 5% CO_2 as previously described [20]. Media changes were performed three times per week. *F.*
690 *hepatica* in culture media are referred to as juveniles.

691

692 RNAi of *fhplk1 in vitro*

693 We generated cDNA from four-week-old juvenile *F. hepatica* by snap freezing 20 juveniles in liquid N_2.
694 Tissues were lysed in a Qiagen tissue lyser with a stainless-steel bead (50 oscillations/sec for 1 min)
695 prior to mRNA extraction with the Dynabeads mRNA Direct Purification Kit (#61011, Thermo Fisher
696 Scientific), DNase treatment (Turbo DNA-free Kit, # AM1907, Thermo Fisher Scientific) and reverse
697 transcription to cDNA using the High-Capacity RNA-to-cDNA Kit (#4387406, Thermo Fisher Scientific).
698 All cDNAs were diluted 1:1 in ddH_2O prior to use. Double-stranded (ds)RNA templates specific to *fhplk1*
699 (FhHiC23_g6132) were generated using 0.4 µM T7-labelled primers (5'-

700 TAATACGACTCACTATAGGGT-3') and the FastStart Taq DNA Polymerase, dNTPack (#4738357001,
701 Millipore Sigma). Primers were designed using Primer3Plus [144], and amplicons were sequenced by
702 Eurofins Genomics (https://eurofinsgenomics.eu/en/) to ensure target specificity. Primers used to
703 generate *fhplk1*-specific dsRNA templates can be found in S10 Table. Negative control dsRNA targeting
704 bacterial neomycin phosphotransferase [U55762] was generated as previously detailed [143]. Template
705 sizes were checked on a 1-2% agarose gel prior to purification using the ChargeSwitch PCR Clean-Up
706 Kit (#CS12000, Thermo Fisher Scientific) and dsRNA generation using the T7 RiboMAX Express RNA
707 System (#P1700, Promega). All dsRNAs were resuspended in ddH_2O with concentrations/purities
708 checked on a DeNovix DS-11 FX spectrophotometer prior to storage as single-use aliquots at -20°C.
709 RNAi treatments were performed by soaking worms in 50 µL of 100 ng/µL dsRNA diluted in RPMI for
710 24 h in 96-well round-bottomed plates under standard conditions detailed above. NEJs were
711 immediately exposed to target-specific dsRNA with juveniles subsequently treated twice a week across
712 four weeks to ensure knockdown [89]. Juveniles were cultured in CS50 between RNAi treatments as
713 standard. All RNAi experiments were carried out in triplicate and included no dsRNA-treatment controls.

714 Juveniles were imaged each week by capturing darkfield videos/images on an Olympus SC50 camera
715 attached to an Olympus SZX10 microscope. Video analyses were performed using the wrMTrck plugin
716 (http://www.phage.dk/plugins/wrmtrck.html, [145]) for ImageJ calibrated to a 1 mm scale. The wrMTrck
717 plugin was used as default except for modifications to minSize (10 pixels), maxSize (1000 pixels),
718 maxVelocity (1000 pixels/frame), AreaChange (200% change in area between frames), Rawdata (2)
719 and benddetect (0). Motility was measured by calculating changes in juvenile length between frames,
720 which provided length change (µm)/minute. Movement of individual juveniles were normalised against
721 mean movement of control juveniles. wrMTrck also provided area (μm^2) measurements for each worm.

722 At the conclusion of RNAi trials juveniles were frozen in liquid N_2 in batches of 20 worms/replicate before
723 cDNA extraction as described above. Quantification of target transcript knockdown was carried out on
724 a Qiagen RotorGene Q 5-plex HRM instrument under the following running conditions: 95°C for 10
725 minutes; 40 cycles @ 95°C for 10 sec, 55°C for 15 sec and 72°C for 20 sec. Melt-curve analyses were
726 enabled to confirm product specificity and qPCR reactions were performed in triplicate using the
727 SensiFast SBYR No-ROX kit (#BIO-98005, Bioline) with final primer concentrations of 200 nM.
728 Glyceraldehyde phosphate dehydrogenase (*fhgapdh*) [AY005475] was used as a housekeeper gene.
729 Alongside *fhplk1*, *fhh2b* [D915_007751] and *fhmlc* [FhHiC23_g308] were amplified as markers for

730 proliferating cells and muscle cells respectively. The oligonucleotide primers used can be found in S10
731 Table. Pfaffl's Augmented ΔΔCt method [146] was used to calculate relative gene expression. Transcript
732 expression was plotted for both target and control-dsRNA-treated groups relative to no dsRNA control.

733

734 Visualisation of proliferative cell activity

735 The thymidine analogue, 5-ethynyl-2-deoxyuridine (EdU; Thermo Fisher Scientific) was used to label
736 nuclei of proliferating neoblast-like cells. A 10 mM stock of EdU was stored at -20°C in PBS. Stock
737 solution was diluted in CS50 to a final working concentration of 500 µM and placed on juveniles for 24
738 h under standard culture conditions. Immediately following EdU exposure worms were flat-fixed under
739 a coverslip in 4% paraformaldehyde (w/v) in PBS (PFA) for 15 minutes, prior to a further 4 h free-fixing
740 in 4% PFA at room temperature while constantly rotating. Worms were permeabilised in 0.5% Triton X-
741 100 in PBS for 30 min at room temperature. EdU detection was achieved using the Click-iT EdU
742 Proliferation Kit for Imaging with the Alexa Fluor 488 dye (#C10337, Thermo Fisher Scientific). Worms
743 were counterstained using 4′,6-diamidino-2-phenylindole (#D1306, DAPI) in PBS for 20 minutes at room
744 temperature prior to mounting in Vectashield (#H-1000-10, Vector Laboratories). A detailed protocol is
745 available at https://dx.doi.org/10.17504/protocols.io.eq2lyjnrrlx9/v1.

746 Samples were imaged on a Lecia TCS SP8 inverted microscope. Z-stacks consisting of 10-15 optical
747 sections between the dorsal and ventral surfaces were captured for each worm and maximally projected
748 for analyses. EdU^+ nuclei counts were performed using the cell counter plugin for ImageJ
749 (https://imagej.nih.gov/ij/plugins/cell-counter.html). Nuclei area (μm^2) measurements were also
750 performed in ImageJ, where images were calibrated to a 50 µm scale.

751

752 RNA-seq and miRNA-seq of *fhplk1* RNAi *F. hepatica* 753 juveniles

754 NEJs were excysted and treated with target-specific dsRNA as described above (~50 worms/replicate
755 split across two wells). Juveniles were treated with dsRNA in RPMI for the final time on day 21 before

being snap frozen in liquid N_2 the following day and stored at -80°C. Total RNA was extracted using Trizol reagent (#15596026, Thermo Fisher Scientific) before being sent to the Genomics Core Technology Unit at Queen's University Belfast (https://www.qub.ac.uk/sites/core-technology-units/Genomics/) for RNA quantification/purity assessment on an AATI fragment analyser prior to library generation using the KAPA mRNA HyperPrep Kit (#KK8580, Roche). Libraries were sequenced (paired end, 2 x 50 bp) on an Illumina Nova seq 6000 SP100 with ~50M reads/sample. Raw read files were uploaded to the European Nucleotide Archive and are available under accession PRJEB85227. Read quality was assessed by fastqc (v.0.11.8) prior to read alignment via HISAT2 (v.2.1.0) against the University of Liverpool *F. hepatica* genome [47] using genome and GTF files available on Wormbase ParaSite (WBPS19, https://parasite.wormbase.org/Fasciola_hepatica_prjeb58756/Info/Index/). Transcripts were assembled in Stringtie (v1.3.6) and a master reference file, excluding isoforms, was generated by merging transcripts from different replicates with the reference genome. This master reference file was used to generate gene counts via Stringtie (v1.3.6) before export into a format readable by DESeq2. 'Novel' transcripts (MSTRGs) generated by Stringtie (v1.3.6) can be found in S2 File.

'Novel' MSTRG sequences with no BLAST hit in the NCBI nr database other than *F. hepatica* and genes with <10 counts across all samples were removed before differential gene expression analysis in R (v4.2.1) by DESeq2 (v.1.34.0). A p-value threshold of 0.001 false discovery rate (FDR) was set to identify differentially expressed genes (DEGs). These DEGs were annotated using the OmicsBox BLAST2GO suite [147] via BLASTx searches against the NCBI non-redundant, landmark and SwissProt databases. Additional BLASTs were carried out against the *S. mansoni* genome (v10, WBPS19, https://parasite.wormbase.org/Schistosoma_mansoni_prjea36577/Info/Index/). Gene ontology (GO) terms were mapped to genes based on BLAST searches and InterproScan results by BLAST2GO annotation software [147] before TOPGO (v.2.36) analysis (parameters: FDR <0.05, method = weight01, statistic = fisher) was carried out on DEGs. KEGG IDs were assigned to transcripts using the eggNOG-mapper [148] tool in OmicsBox (https://www.biobam.com/omicsbox) before gage (v.2.44) and pathview (v.1.34) were used to identify up and downregulated pathways. TOPGO (v.2.36) analysis of *S. mansoni* upregulated genes from Collins et al. [13] was performed by updating all genes to their current IDs and downloading GO terms from Wormbase ParaSite (WBPS19). Parameters were as

785 those used for *F. hepatica* TOPGO analysis. R scripts are available on Github
786 (https://github.com/pmccusker09/F.hepatica_plk1-RNAi_transcriptome_R_analysis.git).

787 Remaining total RNA was processed by the Genomics Core Technology Unit at Queen's University
788 Belfast for miRNA sequencing. Briefly, total RNA was library prepped with the QIASeq miRNA prep kit
789 (#331502, Qiagen) and sequenced on an Illumina Next Seq 2000 with ~8 M single reads per sample
790 (100 bp). Adaptor sequences were trimmed using trimgalore (v.0.4.4) and read quality was assessed
791 by fastqc (v.0.11.8). Raw read files are available under accession PRJEB85228 at the European
792 Nucleotide Archive. Reads were mapped to the University of Liverpool genome downloaded from
793 WormBase ParaSite (WBPS18,
794 https://parasite.wormbase.org/Fasciola_hepatica_prjeb25283/Info/Index/) by bowtie2 (v.2.3.5.1) and
795 miRDeep2 (v.0.1.3) before miRNA counts were generated by miRDeep2 (v.0.1.3), using predicted
796 mature *F. hepatica* miRNAs [132] as a guide. Only counts that mapped to miRNAs previously identified
797 by Herron et al. [132] were taken forward for differential expression analysis by DESeq2 (v.1.34.0) in R
798 (v4.2.1). The targets of differentially expressed miRNAs were predicted by using the same thresholds
799 as Gillan et al. [149]; miRanda (v.; total score >145, energy < -10), RNAhybrid (v.; p<0.1, energy < -22)
800 and PITA (v.; seed sequence of 8 bases with DDG < -10). Target prediction was based on the WBPS18
801 version of the *F. hepatica* genome, as the miRNAs were predicted from that assembly [132], and so
802 RNA-seq analysis was also carried out against this previous version of the genome assembly using the
803 same methodology as detailed above.

804

805 Exposure of juvenile *F. hepatica* to PLK1 inhibitor *in vitro*

806 The PLK inhibitor, BI 2536 (Millipore Sigma) was chosen for testing on juvenile *F. hepatica in vitro*. BI
807 2536 has a strong selectivity for PLK1 and so the amino acid sequence of FhPLK1 was examined to
808 determine if key amino acid residues implicated in drug binding were conserved [150]. The PLK1
809 sequences of *F. hepatica*, *H. sapiens* [P53350], *S. mansoni* [Q5UES2] and *E. multilocularis* [U6HQM1],
810 were aligned using Clustal Omega (https://www.ebi.ac.uk/Tools/msa/clustalo/). Other putative *F.*
811 *hepatica* PLKs identified in our bioinformatic screen were included in the alignment to help predict BI
812 2536 activity. Further BLAST searches against the *F. hepatica* predicted proteomes (WBPS19,

813 https://parasite.wormbase.org) with *H. sapiens* PLKs1-5 [P53350; Q9NYY3; Q9H4B4; O00444;
814 Q496M5] as query sequences did not identify additional *F. hepatica* PLKs.

815 BI 2536 (#A10134, AdooQ Bioscience) and TCBZ (#1681611, Millipore Sigma) were dissolved in 1.7
816 mL NoStick hydrophobic microtubes (#1210-S0, SSIbio) using dimethyl sulphoxide (DMSO). Juvenile
817 *F. hepatica* were washed three times in 1 mL RPMI 1640 to remove excess CS50. They were then
818 transferred to 3.5 cm petri dishes (#82.1135.500, Sarstedt) for exposure in up to 10 µM test compound
819 in a final volume of 3 mL RPMI 1640 for 18 h in standard culture conditions. Compounds were added
820 such that the final DMSO concentration was 0.1% (v/v) in 3 mL RPMI. A vehicle control group (DMSO-
821 treated) was included, with treatments carried out in triplicate. At the conclusion of drug incubations
822 juveniles were subjected to phenotypic observation as detailed above. Where NEJs/juveniles were
823 being further cultured post-exposure, they were washed three times in 1 mL RPMI 1640 to remove
824 excess drug, prior to further culturing as previously described.

825

826 # Statistical Analyses

827 Unless otherwise stated graphs were generated and statistical analyses performed in GraphPad Prism
828 (v10, La Jolla, CA USA). All datasets were tested for normality using either Kolmogorov-Smirnov or
829 Shapiro-Wilk tests. Where data were normally distributed, parametric tests were performed, whereas
830 nonparametric tests were employed where data were non-normally distributed. Relevant post-hoc tests
831 (e.g. Dunn's, Dunnett's and Tukey's multiple comparisons tests) were performed to identify significant
832 differences between multiple groups. Volcano plots were produced using R (v4.2.1). Mean ±standard
833 error mean (SEM) is displayed on graphs unless otherwise stated.

References

1. FAO. Diseases in domestic animals caused by flukes. Food and Agriculture Organisation, Rome. Rome: Food and Agriculture Organisation of the United Nations; 1994.

2. WHO. Integrating neglected tropical diseases into global health and development: fourth WHO report on neglected tropical diseases. Geneva; 2017. Available: https://unitingtocombatntds.org/wp-content/uploads/2017/11/4th_who_ntd_report.pdf

3. Kelley JM, Elliott TP, Beddoe T, Anderson G, Skuce P, Spithill TW. Current threat of triclabendazole resistance in *Fasciola hepatica*. Trends Parasitol. 2016;32: 458–469. doi:10.1016/j.pt.2016.03.002

4. McVeigh P, McCusker P, Robb E, Wells D, Gardiner E, Mousley A, et al. Reasons to Be Nervous about Flukicide Discovery. Trends Parasitol. 2018;34: 184–196. doi:10.1016/j.pt.2017.11.010

5. Boray JC. Studies on experimental infections with fasciola hepatica, with particular reference to acute fascioliasis in sheep. Ann Trop Med Parasitol. 1967;61: 439–450. doi:10.1080/00034983.1967.11686513

6. Fairweather I, Boray JC. Fasciolicides: efficacy, actions, resistance and its management. The Veterinary Journal. 1999;158: 81–112. doi:10.1053/TVJL.1999.0377

7. Wagner DE, Wang IE, Reddien PW. Clonogenic neoblasts are pluripotent adult stem cells that underlie planarian regeneration. Science. 2011;332: 811–816. doi:10.1126/science.1203983

8. Wolff É, Dubois F. Sur la migration des cellules de régénération chez les Planaires. Revue Suisse De Zoologie. 1948;55: 218–227. doi:10.5962/bhl.part.117877

9. Campbell NJ, Gregg P, Kelly JD, Dineen JK. Failure to induce homologous immunity to *Fasciola hepatica* in sheep vaccinated with irradiated metacercariae. Vet Parasitol. 1978;4: 143–152. doi:10.1016/0304-4017(78)90005-5

10. Creaney J, Spithill TW, Thompson CM, Wilson LR, Sandeman RM, Parsons JC. Attempted immunisation of sheep against *Fasciola hepatica* using γ-irradiated metacercariae. Int J Parasitol. 1995;25: 853–856. doi:10.1016/0020-7519(94)00204-2

860 11. Wang B, Collins JJ, Newmark PA. Functional genomic characterization of neoblast-like stem
861 cells in larval *Schistosoma mansoni*. Elife. 2013;2: e00768. doi:10.7554/eLife.00768

862 12. Collins III JJ, Wang B, Lambrus BG, Tharp ME, Iyer H, Newmark PA. Adult somatic stem cells
863 in the human parasite *Schistosoma mansoni*. Nature. 2013;494: 476–9. doi:10.1038/nature11924

864 13. Collins III JJ, Wendt GR, Iyer H, Newmark PA. Stem cell progeny contribute to the schistosome
865 host-parasite interface. Elife. 2016;5: e12473. doi:10.7554/eLife.12473

866 14. Wendt GR, Collins JN, Pei J, Pearson MS, Bennett HM, Loukas A, et al. Flatworm-specific
867 transcriptional regulators promote the specification of tegumental progenitors in *Schistosoma mansoni*.
868 eLife. 2018;7: e33221. doi:10.7554/eLife.33221

869 15. Koziol U, Rauschendorfer T, Zanon Rodríguez L, Krohne G, Brehm K. The unique stem cell
870 system of the immortal larva of the human parasite *Echinococcus multilocularis*. Evodevo. 2014;5: 10.
871 doi:10.1186/2041-9139-5-10

872 16. Rozario T, Quinn EB, Wang J, Davis RE, Newmark PA. Region-specific regulation of stem cell-
873 driven regeneration in tapeworms. Elife. 2019;8: e48958. doi:10.7554/eLife.48958

874 17. Collins JNR, Collins III JJ. Tissue degeneration following loss of *Schistosoma mansoni cbp1* is
875 associated with increased stem cell proliferation and parasite death *in vivo*. PLoS Pathog. 2016;12:
876 e1005963. doi:10.1371/journal.ppat.1005963

877 18. Wendt G, Shiroor DA, Adler CE, Collins III JJ. Convergent evolution of “genome guardian”
878 functions in a parasite-specific p53 homolog. bioRxiv. 2021; 2021.11.28.470261.
879 doi:10.1101/2021.11.28.470261

880 19. Romero AA, Cobb SA, Collins JNR, Kliewer SA, Mangelsdorf DJ, Collins III JJ. The
881 *Schistosoma mansoni* nuclear receptor FTZ-F1 maintains esophageal gland function via transcriptional
882 regulation of meg-8.3. PLoS Pathog. 2021;17: e1010140. doi:10.1371/journal.ppat.1010140

883 20. McCusker P, McVeigh P, Rathinasamy V, Toet H, McCammick E, O’Connor A, et al. Stimulating
884 neoblast-like cell proliferation in juvenile *Fasciola hepatica* supports growth and progression towards
885 the adult phenotype *in vitro*. PLoS Negl Trop Dis. 2016;10: e0004994.
886 doi:10.1371/journal.pntd.0004994

887 21. McCusker P, Clarke NG, Erica G, Armstrong R, McCammick EM, McVeigh P, et al. Neoblast-
888 like stem cells of Fasciola hepatica. PLoS Pathog. 2024;20: e1011903.
889 doi:10.1371/journal.ppat.1011903

890 22. Fabbro D, Cowan-Jacob SW, Moebitz H. Ten things you should know about protein kinases:
891 IUPHAR Review 14. Br J Pharmacol. 2015;172: 2675–2700. doi:10.1111/BPH.13096

892 23. Manning G, Whyte DB, Martinez R, Hunter T, Sudarsanam S. The protein kinase complement
893 of the human genome. Science. 2002;298: 1912–1934. doi:10.1126/science.1075762

894 24. Sharma K, D'Souza RCJ, Tyanova S, Schaab C, Wiśniewski JR, Cox J, et al. Ultradeep Human
895 Phosphoproteome Reveals a Distinct Regulatory Nature of Tyr and Ser/Thr-Based Signaling. Cell Rep.
896 2014;8: 1583–1594. doi:10.1016/j.celrep.2014.07.036

897 25. Wilson LJ, Linley A, Hammond DE, Hood FE, Coulson JM, MacEwan DJ, et al. New
898 Perspectives, opportunities, and challenges in exploring the human protein kinome. Cancer Res.
899 2018;78: 15–29. doi:10.1158/0008-5472.can-17-2291

900 26. Roskoski R. Properties of FDA-approved small molecule protein kinase inhibitors. Pharmacol
901 Res. 2019;144: 19–50. doi:10.1016/j.phrs.2019.03.006

902 27. Gramberg S, Puckelwaldt O, Schmitt T, Lu Z, Haeberlein S. Spatial transcriptomics of a
903 parasitic flatworm provides a molecular map of drug targets and drug resistance genes. Nat Commun.
904 2024;15: 1–19. doi:10.1038/s41467-024-53215-3

905 28. Grevelding CG, Langner S, Dissous C. Kinases: Molecular Stage Directors for Schistosome
906 Development and Differentiation. Trends Parasitol. 2018;34: 246–260. doi:10.1016/j.pt.2017.12.001

907 29. Arora N, Raj A, Anjum F, Kaur R, Rawat SS, Kumar R, et al. Unveiling *Taenia* solium kinome
908 profile and its potential for new therapeutic targets. Expert Rev Proteomics. 2020;17: 85–94.
909 doi:10.1080/14789450.2020.1719835

910 30. Stroehlein AJ, Young ND, Jex AR, Sternberg PW, Tan P, Boag PR, et al. Defining the
911 *Schistosoma haematobium* kinome enables the prediction of essential kinases as anti-schistosome
912 drug targets. Sci Rep. 2015;5. doi:10.1038/srep17759

913 31. Andrade LF, Nahum LA, Avelar LGA, Silva LL, Zerlotini A, Ruiz JC, et al. Eukaryotic Protein
914 Kinases (ePKs) of the Helminth Parasite *Schistosoma mansoni*. BMC Genomics. 2011;12: 1–19.
915 doi:10.1186/1471-2164-12-215

916 32. Sarkar N, Singh A, Kumar P, Kaushik M. Protein kinases: Role of their dysregulation in
917 carcinogenesis, identification and inhibition. Drug Res. 2023;73: 189–199. doi:10.1055/A-1989-1856

918 33. Llamazares S, Moreira A, Tavares A, Girdham C, Spruce BA, Gonzalez C, et al. *polo* encodes
919 a protein kinase homolog required for mitosis in *Drosophila*. Genes Dev. 1991;5: 2153–2165.
920 doi:10.1101/gad.5.12A.2153

921 34. Sunkel CE, Glover DM. Polo, a mitotic mutant of *Drosophila* displaying abnormal spindle poles.
922 J Cell Sci. 1988;89: 25–38. doi:10.1242/jcs.89.1.25

923 35. Kitada K, Johnson AL, Johnston LH, Sugino A. A Multicopy Suppressor Gene of the
924 *Saccharomyces cerevisiae* G1 Cell Cycle Mutant Gene *dbf4* Encodes a Protein Kinase and Is Identified
925 as CDC5. Mol Cell Biol. 1993;13: 4445–4457. doi:10.1128/MCB.13.7.4445-4457.1993

926 36. Ohkura H, Hagan IM, Glover DM. The conserved *Schizosaccharomyces pombe* kinase *plo1*,
927 required to form a bipolar spindle, the actin ring, and septum, can drive septum formation in G1 and G2
928 cells. Genes Dev. 1995;9: 1059–1073. doi:10.1101/GAD.9.9.1059

929 37. Hamanaka R, Maloid S, Smith MR, O CD, Ferris DK, Li DL, et al. Cloning and characterization
930 of human and murine homologues of the *Drosophila* polo serine-threonine kinase. Cell Growth & Differ.
931 1994;5: 249–257.

932 38. Zitouni S, Nabais C, Jana SC, Guerrero A, Bettencourt-Dias M. Polo-like kinases: structural
933 variations lead to multiple functions. Nat Rev Mol Cell Biol. 2014;15: 433–452. doi:10.1038/nrm3819

934 39. Iliaki S, Beyaert R, Afonina IS. Polo-like kinase 1 (PLK1) signaling in cancer and beyond.
935 Biochem Pharmacol. 2021;193: 114747. doi:10.1016/j.bcp.2021.114747

936 40. Long T, Cailliau K, Beckmann S, Browaeys E, Trolet J, Grevelding CG, et al. *Schistosoma*
937 *mansoni* Polo-like kinase 1: A mitotic kinase with key functions in parasite reproduction. Int J Parasitol.
938 2010;40: 1075–1086. doi:10.1016/j.ijpara.2010.03.002

939 41. Dissous C, Grevelding CG, Long T. *Schistosoma mansoni* polo-like kinases and their function
940 in control of mitosis and parasite reproduction. An Acad Bras Cienc. 2011;83: 627–635.
941 doi:10.1590/S0001-37652011000200022

942 42. Long T, Neitz RJ, Beasley R, Kalyanaraman C, Suzuki BM, Jacobson MP, et al. Structure-
943 Bioactivity Relationship for Benzimidazole Thiophene Inhibitors of Polo-Like Kinase 1 (PLK1), a
944 Potential Drug Target in *Schistosoma mansoni*. PLoS Negl Trop Dis. 2016;10: e0004356.
945 doi:10.1371/journal.pntd.0004356

946 43. Schubert A, Koziol U, Cailliau K, Vanderstraete M, Dissous C, Brehm K. Targeting
947 *Echinococcus multilocularis* stem cells by inhibition of the polo-like kinase *Emplk1*. PLoS Negl Trop Dis.
948 2014;8: e2870. doi:10.1371/journal.pntd.0002870

949 44. Houhou H, Puckelwaldt O, Strube C, Haeberlein S. Reference gene analysis and its use for
950 kinase expression profiling in *Fasciola hepatica*. Sci Rep. 2019;9: 15867. doi:10.1038/s41598-019-
951 52416-x

952 45. Morawietz CM, Houhou H, Puckelwaldt O, Hehr L, Dreisbach D, Mokosch A, et al. Targeting
953 kinases in *Fasciola hepatica*: anthelminthic effects and tissue distribution of selected kinase inhibitors.
954 Front Vet Sci. 2020;7: 611270. doi:10.3389/fvets.2020.611270

955 46. Robb E, McCammick EM, Wells D, McVeigh P, Gardiner E, Armstrong R, et al. Transcriptomic
956 analysis supports a role for the nervous system in regulating growth and development of *Fasciola*
957 *hepatica* juveniles. PLoS Negl Trop Dis. 2022;16: e0010854. doi:10.1371/journal.pntd.0010854

958 47. Cwiklinski K, Dalton JP, Dufresne PJ, La Course J, Williams DJ, Hodgkinson J, et al. The
959 *Fasciola hepatica* genome: gene duplication and polymorphism reveals adaptation to the host
960 environment and the capacity for rapid evolution. Genome Biol. 2015;16: 71. doi:10.1186/s13059-015-
961 0632-2

962 48. Plowman GD, Sudarsanam S, Bingham J, Whyte D, Hunter T. The protein kinases of
963 *Caenorhabditis elegans*: A model for signal transduction in multicellular organisms. Proc Natl Acad Sci
964 USA. 1999;96: 13603–13610. doi:10.1073/pnas.96.24.13603

965 49. Manning G, Plowman GD, Hunter T, Sudarsanam S. Evolution of protein kinase signaling from
966 yeast to man. Trends Biochem Sci. 2002;27: 514–520. doi:10.1016/S0968-0004(02)02179-5

967 50. Skelding KA, Rostas JAP. The Role of Molecular Regulation and Targeting in Regulating
968 Calcium/Calmodulin Stimulated Protein Kinases. Adv Exp Med Biol. 2012;740: 703–730.
969 doi:10.1007/978-94-007-2888-2_31

970 51. You H, McManus DP, Hu W, Smout MJ, Brindley PJ, Gobert GN. Transcriptional Responses of
971 *In Vivo* Praziquantel Exposure in Schistosomes Identifies a Functional Role for Calcium Signalling
972 Pathway Member CamKII. PLoS Pathog. 2013;9: e1003254. doi:10.1371/journal.ppat.1003254

973 52. Hirst NL, Lawton SP, Walker AJ. CaMKII regulates neuromuscular activity and survival of the
974 human blood fluke *Schistosoma mansoni*. Sci Rep. 2022;12: 1–14. doi:10.1038/s41598-022-23962-8

975 53. Chowdhury I, Dashi G, Keskitalo S. CMGC Kinases in Health and Cancer. Cancers 2023, Vol
976 15, Page 3838. 2023;15: 3838. doi:10.3390/cancers15153838

977 54. Puckelwaldt O, Gramberg S, Ajmera S, Koepke J, Samakovlis C, Haeberlein S. Single-cell
978 transcriptomics identifies a p21-activated kinase important for survival of the zoonotic parasite *Fasciola*
979 *hepatica*. bioRxiv. 2024; 2024.03.26.586785. doi:10.1101/2024.03.26.586785

980 55. Kanev GK, de Graaf C, de Esch IJP, Leurs R, Würdinger T, Westerman BA, et al. The
981 Landscape of Atypical and Eukaryotic Protein Kinases. Trends Pharmacol Sci. 2019;40: 818–832.
982 doi:10.1016/j.tips.2019.09.002

983 56. Zaru R, Magrane M, O'Donovan C, Bateman A, Martin MJ, Alpi E, et al. From the research
984 laboratory to the database: the *Caenorhabditis elegans* kinome in UniProtKB. Biochemical Journal.
985 2017;474: 493–515. doi:10.1042/BCJ20160991

986 57. Hua H, Kong Q, Zhang H, Wang J, Luo T, Jiang Y. Targeting mTOR for cancer therapy. J
987 Hematol Oncol. 2019;12: 1–19. doi:10.1186/S13045-019-0754-1

988 58. Weber AM, Ryan AJ. ATM and ATR as therapeutic targets in cancer. Pharmacol Ther. 2015;149:
989 124–138. doi:10.1016/j.pharmthera.2014.12.001

990 59. Burke JE, Triscott J, Emerling BM, Hammond GRV. Beyond PI3Ks: targeting phosphoinositide
991 kinases in disease. Nature Reviews Drug Discovery 2022 22:5. 2022;22: 357–386.
992 doi:10.1038/s41573-022-00582-5

993 60. Malumbres M, Barbacid M. Cell cycle, CDKs and cancer: a changing paradigm. Nat Rev
994 Cancer. 2009;9: 153–166. doi:10.1038/nrc2602

995 61. Wang XQ, Lo CM, Chen L, Ngan ESW, Xu A, Poon RYC. CDK1-PDK1-PI3K/Akt signaling
996 pathway regulates embryonic and induced pluripotency. Cell Death Differ. 2017;24: 38–48.
997 doi:10.1038/cdd.2016.84

998 62. Santamaría D, Barrière C, Cerqueira A, Hunt S, Tardy C, Newton K, et al. Cdk1 is sufficient to
999 drive the mammalian cell cycle. Nature 2007;448: 811–815. doi:10.1038/nature06046

1000 63. Babina IS, Turner NC. Advances and challenges in targeting FGFR signalling in cancer. Nat
1001 Rev Cancer. 2017;17: 318–332. doi:10.1038/nrc.2017.8

1002 64. Förster S, Koziol U, Schäfer T, Duvoisin R, Cailliau K, Vanderstraete M, et al. The role of
1003 fibroblast growth factor signalling in *Echinococcus multilocularis* development and host-parasite
1004 interaction. PLoS Negl Trop Dis. 2019;13: e0006959. doi:10.1371/journal.pntd.0006959

1005 65. Du X, McManus DP, French JD, Collinson N, Sivakumaran H, MacGregor SR, et al. CRISPR
1006 interference for sequence-specific regulation of fibroblast growth factor receptor A in *Schistosoma*
1007 *mansoni*. Front Immunol. 2023;13: 1105719. doi:10.3389/fimmu.2022.1105719/bibtex

1008 66. Roskoski R. Properties of FDA-approved small molecule protein kinase inhibitors: A 2021
1009 update. Pharmacol Res. 2021;165: 105463. doi:10.1016/j.phrs.2021.105463

1010 67. Strebhardt K, Ullrich A. Targeting polo-like kinase 1 for cancer therapy. Nat Rev Cancer. 2006;6:
1011 321–330. doi:10.1038/nrc1841

1012 68. Hanks SK, Hunter T. The eukaryotic protein kinase superfamily: kinase (catalytic) domain
1013 structure and classification1. The FASEB Journal. 1995;9: 576–596. doi:10.1096/fasebj.9.8.7768349

1014 69. Seki A, Coppinger JA, Jang CY, Yates JR, Fang G. Bora and the kinase Aurora A cooperatively
1015 activate the kinase Plk1 and control mitotic entry. Science. 2008;320: 1655–1658.
1016 doi:10.1126/science.1157425

1017 70. Elia AEH, Cantley LC, Yaffe MB. Proteomic screen finds pSer/pThr-binding domain localizing
1018 Plk1 to mitotic substrates. Science. 2003;299: 1228–1231. doi:10.1126/science.1079079

1019 71. Elia AEH, Rellos P, Haire LF, Chao JW, Ivins FJ, Hoepker K, et al. The molecular basis for
1020 phosphodependent substrate targeting and regulation of Plks by the Polo-box domain. Cell. 2003;115:
1021 83–95. doi:10.1016/S0092-8674(03)00725-6

1022 72. Wang J, Chen R, Collins III JJ. Systematically improved *in vitro* culture conditions reveal new
1023 insights into the reproductive biology of the human parasite *Schistosoma mansoni*. PLoS Biol. 2019;17:
1024 e3000254. doi:10.1371/journal.pbio.3000254

1025 73. Hanna R. *Fasciola hepatica*: Histology of the Reproductive Organs and Differential Effects of
1026 Triclabendazole on Drug-Sensitive and Drug-Resistant Fluke Isolates and on Flukes from Selected
1027 Field Cases. Pathogens. 2015;4: 431–456. doi:10.3390/pathogens4030431

1028 74. Björkman N, Thorsell W. On the ultrastructure of the ovary of the liver fluke (*Fasciola hepatica*
1029 L.). Zeitschrift für Zellforschung und Mikroskopische Anatomie. 1964;63: 538–549.
1030 doi:10.1007/bf00339489/metrics

1031 75. Marzluff WF, Wagner EJ, Duronio RJ. Metabolism and regulation of canonical histone mRNAs:
1032 life without a poly(A) tail. Nat Rev Genet. 2008;9: 843–854. doi:10.1038/nrg2438

1033 76. Pettitt J, Crombie C, Schümperli D, Müller B. The *Caenorhabditis elegans* histone hairpin-
1034 binding protein is required for core histone gene expression and is essential for embryonic and
1035 postembryonic cell division. J Cell Sci. 2002;115: 857–866. doi:10.1242/JCS.115.4.857

1036 77. Sullivan E, Santiago C, Parker ED, Dominski Z, Yang X, Lanzotti DJ, et al. *Drosophila* stem
1037 loop binding protein coordinates accumulation of mature histone mRNA with cell cycle progression.
1038 Genes Dev. 2001;15: 173–187. doi:10.1101/gad.862801

1039 78. Solana J, Kao D, Mihaylova Y, Jaber-Hijazi F, Malla S, Wilson R, et al. Defining the molecular
1040 profile of planarian pluripotent stem cells using a combinatorial RNAseq, RNA interference and
1041 irradiation approach. Genome Biol. 2012;13: 1–23. doi:10.1186/gb-2012-13-3-r19

1042 79. Spänkuch-Schmitt B, Bereiter-Hahn J, Kaufmann M, Strebhardt K. Effect of RNA Silencing of
1043 Polo-Like Kinase-1 (PLK1) on Apoptosis and Spindle Formation in Human Cancer Cells. J Natl Cancer
1044 Inst. 2002;94: 1863–1877. doi:10.1093/JNCI/94.24.1863

1045 80. McCarroll JA, Dwarte T, Baigude H, Dang J, Yang L, Erlich RB, et al. Therapeutic targeting of
1046 polo-like kinase 1 using RNA-interfering nanoparticles (iNOPs) for the treatment of non-small cell lung
1047 cancer. Oncotarget. 2015;6: 12020–12034. doi:10.18632/oncotarget.2664

1048 81. Sampath P, Pritchard DK, Pabon L, Reinecke H, Schwartz SM, Morris DR, et al. A Hierarchical
1049 Network Controls Protein Translation during Murine Embryonic Stem Cell Self-Renewal and
1050 Differentiation. Cell Stem Cell. 2008;2: 448–460. doi:10.1016/j.stem.2008.03.013

1051 82. Saba JA, Liakath-Ali K, Green R, Watt FM. Translational control of stem cell function. Nat Rev
1052 Mol Cell Biol. 2021;22: 671–690. doi:10.1038/s41580-021-00386-2

1053 83. Larson DE, Xie W, Glibetic M, O'Mahony D, Sells BH, Rothblum LI. Coordinated decreases in
1054 rRNA gene transcription factors and rRNA synthesis during muscle cell differentiation. PNAS. 1993;90:
1055 7933–7936. doi:10.1073/PNAS.90.17.7933

1056 84. Cong Y, Yang H, Zhang P, Xie Y, Cao X, Zhang L. Transcriptome Analysis of the Nematode
1057 *Caenorhabditis elegans* in Acidic Stress Environments. Front Physiol. 2020;11: 1107.
1058 doi:10.3389/fphys.2020.01107/full

1059 85. Jasmer DP, Rosa BA, Mitreva M. Cell death and transcriptional responses induced in larvae of
1060 the nematode *Haemonchus contortus* by toxins/toxicants with broad phylogenetic efficacy.
1061 Pharmaceuticals. 2021;14: 598. doi:10.3390/ph14070598

1062 86. Chen J. The Cell-Cycle Arrest and Apoptotic Functions of p53 in Tumor Initiation and
1063 Progression. Cold Spring Harb Perspect Med. 2016;6: a026104. doi:10.1101/cshperspect.A026104

1064 87. Duffy MJ, Synnott NC, Crown J. Mutant p53 as a target for cancer treatment. Eur J Cancer.
1065 2017;83: 258–265. doi:10.1016/J.EJCA.2017.06.023

1066 88. Fei L, Xu H. Role of MCM2-7 protein phosphorylation in human cancer cells. Cell Biosci.
1067 2018;8: 1–8. doi:10.1186/S13578-018-0242-2

1068 89. McCusker P, Hussain W, McVeigh P, McCammick E, Clarke NG, Robb E, et al. RNA
1069 interference dynamics in juvenile *Fasciola hepatica* are altered during *in vitro* growth and development.
1070 Int J Parasitol Drugs Drug Resist. 2020;14: 46–55. doi:10.1016/j.ijpddr.2020.08.004

1071 90. Vigneron S, Brioudes E, Burgess A, Labbé JC, Lorca T, Castro A. Greatwall maintains mitosis
1072 through regulation of PP2A. EMBO Journal. 2009;28: 2786–2793. doi:10.1038/emboj.2009.228

1073 91. Im JS, Ki SH, Farina A, Jung DS, Hurwitz J, Lee JK. Assembly of the Cdc45-Mcm2-7-GINS
1074 complex in human cells requires the Ctf4/And-1, RecQL4, and Mcm10 proteins. PNAS. 2009;106:
1075 15628–15632. doi:10.1073/pnas.0908039106

1076 92. Komorowska K, Doyle A, Wahlestedt M, Subramaniam A, Debnath S, Chen J, et al. Hepatic
1077 Leukemia Factor Maintains Quiescence of Hematopoietic Stem Cells and Protects the Stem Cell Pool
1078 during Regeneration. Cell Rep. 2017;21: 3514–3523. doi:10.1016/j.celrep.2017.11.084

1079 93. Stoll K, Bergmann M, Spiliotis M, Brehm K. A MEKK1 – JNK mitogen activated kinase (MAPK)
1080 cascade module is active in *Echinococcus multilocularis* stem cells. PLoS Negl Trop Dis. 2021;15:
1081 e0010027. doi:10.1371/journal.pntd.0010027

1082 94. Beyer EC, Berthoud VM. Gap junction gene and protein families: Connexins, innexins, and
1083 pannexins. Biochim Biophys Acta Biomembr. 2018;1860: 5–8. doi:10.1016/j.bbamem.2017.05.016

1084 95. Nogi T, Levin M. Characterization of innexin gene expression and functional roles of gap-
1085 junctional communication in planarian regeneration. Dev Biol. 2005;287: 314–335.
1086 doi:10.1016/j.ydbio.2005.09.002

1087 96. Oviedo NJ, Morokuma J, Walentek P, Kema IP, Gu MB, Ahn JM, et al. Long-range neural and
1088 gap junction protein-mediated cues control polarity during planarian regeneration. Dev Biol. 2010;339:
1089 188–199. doi:10.1016/j.ydbio.2009.12.012

1090 97. Oviedo NJ, Levin M. smedinx-11 is a planarian stem cell gap junction gene required for
1091 regeneration and homeostasis. Development. 2007;134: 3121–3131. doi:10.1242/DEV.006635

1092 98. Maule AG, Marks NJ, Day TA. Signalling Molecules and Nerve-Muscle Function. In: Maule AG,
1093 Marks N, editors. Parasitic Flatworms: Molecular Biology, Biochemistry, Immunology and Physiology.
1094 CABI; 2006. pp. 369–381.

1095 99. El-Shehabi F, Ribeiro P. Histamine signalling in *Schistosoma mansoni*: Immunolocalisation and
1096 characterisation of a new histamine-responsive receptor (SmGPR-2). Int J Parasitol. 2010;40: 1395–
1097 1406. doi:10.1016/J.ijpara.2010.04.006

1098 100. Sukhodeo SC, Sangster NC, Mettrick DF. Effects of cholinergic drugs on longitudinal muscle
1099 contractions of *Fasciola hepatica*. J Parasitol. 1986;72: 858–864. doi:10.2307/3281834

1100 101. Sukhdeo MVK, Mettrick DF. The behavior of juvenile *Fasciola hepatica*. J Parasitol. 1986;72:
1101 492–497. doi:10.2307/3281496

1102 102. Fanburg BL, Lee SL. A new role for an old molecule: serotonin as a mitogen. Am J Physiol.
1103 1997;272: L795-806. doi:10.1152/ajplung.1997.272.5.L795

1104 103. Franquinet R, Martelly I. Effects of serotonin and catecholamines on RNA synthesis in
1105 planarians; *in vitro* and *in vivo* studies. Cell Differ. 1981;10: 201–209. doi:10.1016/0045-6039(81)90002-
1106 6

1107 104. Taft AS, Norante FA, Yoshino TP. The identification of inhibitors of *Schistosoma mansoni*
1108 miracidial transformation by incorporating a medium-throughput small-molecule screen. Exp Parasitol.
1109 2010;125: 84–94. doi:10.1016/j.exppara.2009.12.021

1110 105. Kawamoto F, Shozawa A, Kumada N, Kojima K. Possible roles of cAMP and Ca2+ in the
1111 regulation of miracidial transformation in *Schistosoma mansoni*. Parasitol Res. 1989;75: 368–374.
1112 doi:10.1007/BF00931132

1113 106. Boyle JP, Zaide J V., Yoshino TP. *Schistosoma mansoni*: Effects of Serotonin and Serotonin
1114 Receptor Antagonists on Motility and Length of Primary Sporocysts *in vitro*. Exp Parasitol. 2000;94:
1115 217–226. doi:10.1006/expr.2000.4500

1116 107. Herz M, Brehm K. Serotonin stimulates *Echinococcus multilocularis* larval development. Parasit
1117 Vectors. 2021;14: 1–12. doi:10.1186/S13071-020-04533-0

1118 108. Alqahtani S, Butcher MC, Ramage G, Dalby MJ, McLean W, Nile CJ. Acetylcholine Receptors
1119 in Mesenchymal Stem Cells. Stem Cells Dev. 2023;32: 47–59. doi:10.1089/SCD.2022.0201

1120 109. Basu S, Dasgupta PS. Role of dopamine in malignant tumor growth. Endocrine. 2000;12: 237–
1121 241. doi:10.1385/endo:12:3:237

1122 110. Lee I, Knickerbocker AC, Depew CR, Martin E, Dicent J, Miller GW, et al. Effect of altered
1123 production and storage of dopamine on development and behavior in *C. elegans*. bioRxiv. 2023;
1124 2023.10.07.561350. doi:10.1101/2023.10.07.561350

1125 111. Neckameyer WS. Multiple Roles for Dopamine in *Drosophila* Development. Dev Biol. 1996;176:
1126 209–219. doi:10.1006/dbio.1996.0128

1127 112. Taft AS, Norante FA, Yoshino TP. The identification of inhibitors of *Schistosoma mansoni*
1128 miracidial transformation by incorporating a medium-throughput small-molecule screen. Exp Parasitol.
1129 2010;125: 84. doi:10.1016/j.exppara.2009.12.021

1130 113. Rand JB, Russell RL. Choline acetyltransferase-deficient mutants of the nematode
1131 *Caenorhabditis elegans*. Genetics. 1984;106: 227–248. doi:10.1093/genetics/106.2.227

1132 114. Zachary I, Woll PJ, Rozengurt E. A role for neuropeptides in the control of cell proliferation. Dev
1133 Biol. 1987;124: 295–308. doi:10.1016/0012-1606(87)90483-0

1134 115. Kreshchenko ND. Functions of flatworm neuropeptides NPF, GYIRF and FMRF in course of
1135 pharyngeal regeneration of anterior body fragments of planarian, *Girardia tigrina*. Acta Biol Hung.
1136 2008;59: 199–207. doi:10.1556/ABiol.59.2008.Suppl.29

1137 116. Collins III JJ, Hou X, Romanova E V., Lambrus BG, Miller CM, Saberi A, et al. Genome-Wide
1138 Analyses Reveal a Role for Peptide Hormones in Planarian Germline Development. PLoS Biol. 2010;8:
1139 e1000509. doi:10.1371/journal.pbio.1000509

1140 117. Saberi A, Jamal A, Beets I, Schoofs L, Newmark PA. GPCRs Direct Germline Development and
1141 Somatic Gonad Function in Planarians. PLoS Biol. 2016;14: e1002457.
1142 doi:10.1371/journal.pbio.1002457

1143 118. Bagurija' J, Salo E, Romero R. Effects of activators and antagonists of the neuropeptides
1144 substance P and substance K on cell proliferation in planarians. Int J Dev Biol. 1989;33: 261–264.

1145 119. Li X, Weth O, Haimann M, Möscheid MF, Huber TS, Grevelding CG, et al. Rhodopsin orphan
1146 GPCR20 interacts with neuropeptides and directs growth, sexual differentiation, and egg production in
1147 female *Schistosoma mansoni*. Microbiol Spectr. 2023;12: e0219323 doi:10.1128/spectrum.02193-23

1148 120. Almuedo-Castillo M, Sureda-Gómez M, Adell T. Wnt signaling in planarians: New answers to
1149 old questions. International Journal of Developmental Biology. 2012;56: 53–65.
1150 doi:10.1387/ijdb.113451ma

121. Ye Z, Xu J, Feng X, Jia Y, Fu Z, Hong Y, et al. Spatiotemporal expression pattern of *Sjfz7* and its expression comparison with other frizzled family genes in developmental stages of *Schistosoma japonicum*. Gene Expression Patterns. 2019;32: 44–52. doi:10.1016/j.gep.2019.02.005

122. Cheng G, Li X, Qin F, Xu R, Zhang Y, Liu J, et al. Functional analysis of the *Frzb2* gene in *Schistosoma japonicum*. Vet Res. 2019;50: 1–11. doi:10.1186/S13567-019-0716-1

123. Koziol U, Jarero F, Olson PD, Brehm K. Comparative analysis of Wnt expression identifies a highly conserved developmental transition in flatworms. BMC Biol. 2016;14: 1–16. doi:10.1186/s12915-016-0233-x

124. Gurley KA, Elliott SA, Simakov O, Schmidt HA, Holstein TW, Alvarado AS. Expression of secreted Wnt pathway components reveals unexpected complexity of the planarian amputation response. Dev Biol. 2010;347: 24–39. doi:10.1016/j.ydbio.2010.08.007

125. Adell T, Salò E, Boutos M, Bartscherer K. Smed-*Evi/Wntless* is required for β-catenin-dependent and-independent processes during planarian regeneration. Development. 2009;136: 905–910. doi:10.1242/DEV.033761

126. Li HF, Wang XB, Jin YP, Xia YX, Feng XG, Yang JM, et al. *Wnt4*, the first member of the *Wnt* family identified in Schistosoma japonicum, regulates worm development by the canonical pathway. Parasitol Res. 2010;107: 795–805. doi:10.1007/S00436-010-1933-8

127. Kobayashi C, Saito Y, Ogawa K, Agata K. Wnt signaling is required for antero-posterior patterning of the planarian brain. Dev Biol. 2007;306: 714–724. doi:10.1016/j.ydbio.2007.04.010

128. Armstrong R, Marks NJ, Geary TG, Harrington J, Selzer PM, Maule AG. Wnt/β-catenin signalling underpins juvenile *Fasciola hepatica* growth and development. PLoS Pathog. 2025;21: e1012562. doi: 10.1371/journal.ppat.1012562

129. Lingueglia E, Champigny G, Lazdunski M, Barbry P. Cloning of the amiloride-sensitive FMRFamide peptide-gated sodium channel. Nature 1995;378: 730–733. doi:10.1038/378730a0

130. Baguñà J. The planarian neoblast: the rambling history of its origin and some current black boxes. Int J Dev Biol. 2012;56: 19–37. doi:10.1387/ijdb.113463jb

1177 131. Yang D, Zhou Q, Labroska V, Qin S, Darbalaei S, Wu Y, et al. G protein-coupled receptors:
1178 structure- and function-based drug discovery. Signal Transduct Target Ther. 2021;6: 1–27.
1179 doi:10.1038/s41392-020-00435-w

1180 132. Herron CM, O'Connor A, Robb E, McCammick E, Hill C, Marks NJ, et al. Developmental
1181 Regulation and Functional Prediction of microRNAs in an Expanded *Fasciola hepatica* miRNome. Front
1182 Cell Infect Microbiol. 2022;12. doi:10.3389/fcimb.2022.811123

1183 133. Kothe M, Kohls D, Low S, Coli R, Rennie GR, Feru F, et al. Selectivity-determining Residues in
1184 Plk1. Chem Biol Drug Des. 2007;70: 540–546. doi:10.1111/J.1747-0285.2007.00594.X

1185 134. Steegmaier M, Hoffmann M, Baum A, Lénárt P, Petronczki M, Krššák M, et al. BI 2536, a Potent
1186 and Selective Inhibitor of Polo-like Kinase 1, Inhibits Tumor Growth *In Vivo*. Curr Biol. 2007;17: 316–
1187 322. doi:10.1016/j.cub.2006.12.037

1188 135. Long T, Vanderstraete M, Cailliau K, Morel M, Lescuyer A, Gouignard N, et al. *SmSak*, the
1189 second polo-like kinase of the helminth parasite *Schistosoma mansoni*: conserved and unexpected
1190 roles in meiosis. PLoS One. 2012;7: e40045. doi:10.1371/journal.pone.0040045

1191 136. Bennett CEE. Surface Features, Sensory Structures, and Movement of the Newly Excysted
1192 Juvenile *Fasciola hepatica* L. J Parasitol. 1975;61: 886–891.

1193 137. Taylor S, Peters JM. Polo and Aurora kinases — lessons derived from chemical biology. Curr
1194 Opin Cell Biol. 2008;20: 77–84. doi:10.1016/J.CEB.2007.11.008

1195 138. Gelmedin V, Dissous C, Grevelding CG. Re-positioning protein-kinase inhibitors against
1196 schistosomiasis. Future Med Chem. 2015;7: 737–752. doi:10.4155/fmc.15.31

1197 139. McNulty SN, Tort JF, Rinaldi G, Fischer K, Rosa BA, Smircich P, et al. Genomes of *Fasciola*
1198 *hepatica* from the Americas Reveal Colonization with *Neorickettsia* Endobacteria Related to the Agents
1199 of Potomac Horse and Human Sennetsu Fevers. PLoS Genet. 2017;13: e1006537.
1200 doi:10.1371/journal.pgen.1006537

1201 140. Lee RYN, Howe KL, Harris TW, Arnaboldi V, Cain S, Chan J, et al. WormBase 2017: molting
1202 into a new stage. Nucleic Acids Res. 2018;46: D869–D874. doi:10.1093/nar/gkx998

1203 141. Tancred Frickey, Andrei Lupas. CLANS: a Java application for visualizing protein families based
1204 on pairwise similarity. Bioinformatics. 2004;20: 3702–3704. doi:10.1093/bioinformatics/BTH444

1205 142. Tamura K, Stecher G, Kumar S. MEGA11: Molecular Evolutionary Genetics Analysis Version
1206 11. Mol Biol Evol. 2021;38: 3022–3027. doi:10.1093/molbev/msab120

1207 143. McVeigh P, McCammick EM, McCusker P, Morphew RM, Mousley A, Abidi A, et al. RNAi
1208 dynamics in juvenile *Fasciola* spp. liver flukes reveals the persistence of gene silencing *in vitro*. PLoS
1209 Negl Trop Dis. 2014;8: e3185. doi:10.1371/journal.pntd.0003185

1210 144. Untergasser A, Nijveen H, Rao X, Bisseling T, Geurts R, Leunissen JAM. Primer3Plus, an
1211 enhanced web interface to Primer3. Nucleic Acids Res. 2007;35: W71-4. doi:10.1093/nar/gkm306

1212 145. Schneider CA, Rasband WS, Eliceiri KW. NIH Image to ImageJ: 25 years of image analysis.
1213 Nat Methods 2012 9:7. 2012;9: 671–675. doi:10.1038/nmeth.2089

1214 146. Pfaffl MW. A new mathematical model for relative quantification in real-time RT-PCR. Nucleic
1215 Acids Res. 2001;29: e45. doi:10.1093/nar/29.9.e45

1216 147. Götz S, García-Gómez JM, Terol J, Williams TD, Nagaraj SH, Nueda MJ, et al. High-throughput
1217 functional annotation and data mining with the Blast2GO suite. Nucleic Acids Res. 2008;36: 3420–3435.
1218 doi:10.1093/nar/gkn176

1219 148. Cantalapiedra CP, Herṇandez-Plaza A, Letunic I, Bork P, Huerta-Cepas J. eggNOG-mapper v2:
1220 Functional Annotation, Orthology Assignments, and Domain Prediction at the Metagenomic Scale. Mol
1221 Biol Evol. 2021;38: 5825–5829. doi:10.1093/molbev/msab293

1222 149. Gillan V, Maitland K, Laing R, Gu H, Marks ND, Winter AD, et al. Increased expression of a
1223 microRNA correlates with anthelmintic resistance in parasitic nematodes. Front Cell Infect Microbiol.
1224 2017;7: 292984. doi:10.3389/FCIMB.2017.00452

1225 150. Kothe M, Kohls D, Low S, Coli R, Rennie GR, Feru F, et al. Selectivity-determining Residues in
1226 Plk1. Chem Biol Drug Des. 2007;70: 540–546. doi:10.1111/J.1747-0285.2007.00594.X

1227

1228 # Supplementary Information

1229 **S1 Fig. Identification and compilation of *Fasciola hepatica* protein kinases.**

1230 (A) Bioinformatics pipeline used to identify putative protein kinases in *F. hepatica* through HMM
1231 searches, BLAST identification, manual curation and CLANs analysis. (B) Proportions (%) of eukaryotic
1232 protein kinase families in *F. hepatica*, *Schistosoma mansoni*, *Schistosoma haematobium*,
1233 *Caenorhabditis elegans*, *Haemonchus contortus*, *Drosophila melanogaster* and *Homo sapiens*
1234 kinomes. (C) Maximum-likelihood tree (WAG +G + F model) with 100 bootstraps of predicted *F. hepatica*
1235 atypical protein kinases; colours denote family.

1236 **S2 Fig. Cell proliferation does not recover up to a week after *fhplk1* dsRNA exposure in juvenile**
1237 ***Fasciola hepatica in vitro*.**

1238 (A) Timelines for experiments show juvenile *F. hepatica* were treated for four weeks with either control
1239 dsRNA or *fhplk1* dsRNA before a final week in culture with no dsRNA treatments prior to EdU exposure
1240 and subsequent staining. (B) Confocal images of EdU staining (green) in juvenile *F. hepatica* treated
1241 according to adjacent timelines show that EdU^+ nuclei did not recover after *fhplk1* dsRNA exposures
1242 were stopped; scale bar = 100 μm, DAPI counterstain (magenta). (C) Mean # EdU^+ nuclei ±SEM in
1243 juvenile *F. hepatica* treated according to adjacent timelines shows complete loss of EdU^+ nuclei in *fhplk1*
1244 dsRNA-treated worms, even after culture for one week post drug exposure.

1245 **S3 Fig. Downregulation of cell cycle and ribosome associated transcripts in *fhplk1*-RNAi juvenile**
1246 ***Fasciola hepatica*.**

1247 (A) Mean area (μm^2) ±SEM of juvenile *F. hepatica* used in transcriptomics shows reduced growth rate
1248 in worms repeatedly treated with *fhplk1* dsRNA for three weeks. (B) Confocal images of EdU staining
1249 (green) in juvenile *F. hepatica* used for transcriptomics confirmed ablation of EdU^+ nuclei after repeated
1250 treatment with *fhplk1* dsRNA for three weeks. (C) GO terms (top 10 molecular function and top 10
1251 cellular component) overrepresented among downregulated transcripts following *fhplk1* dsRNA
1252 treatment in juvenile *F. hepatica*. (D) KEGG pathways significantly downregulated following *fhplk1*-RNAi
1253 in juvenile *F. hepatica* are associated with ribosomal components and cell cycle/proliferation. (E)
1254 Integrative genomics viewer (IGV) screenshot of transcriptomic reads in all RNA sequenced samples
1255 mapped against the *F. hepatica fhplk1* gene shows reads across the whole gene in control dsRNA
1256 samples, but a spike in reads around the dsRNA amplicon region in *fhplk1* dsRNA samples (red box to

1257 highlight). (F) IGV screenshots of beginning and end of *fhplk1* dsRNA amplicon region show that reads
1258 in *fhplk1* dsRNA samples begin and end where forward ('F' green) and reverse ('R' pink) amplicon
1259 primers are located.

1260 **S4 Fig. Upregulated cell signalling and receptors/ion channel subunits in *fhplk1*-RNAi *Fasciola***
1261 ***hepatica* juveniles.**
1262 (A) GO terms (top 10 molecular function and top 10 cellular component) overrepresented in transcripts
1263 upregulated following *fhplk1*-RNAi in *F. hepatica* juveniles. (B) KEGG pathways associated with inter-
1264 cell signalling (gap junction, neural synapses and signalling pathways) significantly upregulated
1265 following *fhplk1*-RNAi in juvenile *F. hepatica*. (C) KEGG Gap Junction pathway following *fhplk1*-RNAi
1266 shows upregulation of diverse pathway components (red = upregulated; grey = no change; blue =
1267 downregulated; white = unassigned KEGG ID). (D) KEGG GABAergic synapse pathway following
1268 *fhplk1*-RNAi shows upregulation of diverse pathway components (red = upregulated; grey = no change;
1269 blue = downregulated; white = unassigned KEGG ID). (E) Top 10 Biological process GO terms
1270 overrepresented in significantly upregulated transcripts in both *fhplk1*-RNAi and slower growing *in vitro*
1271 worms (S6 Table) are associated with neuronal signalling. (F) DAPI (nuclei) stain coverage (as a
1272 percentage of the total area of the worm) in control-dsRNA treated and *fhplk1*-dsRNA treated worms
1273 shows ~20% reduction. (G) Significantly upregulated receptors/channel subunits following *fhplk1*-RNAi.

1274 **S5 Fig. GO terms of predicted targets for differentially expressed miRNAs following *fhplk1*-RNAi**
1275 **in *Fasciola hepatica* juveniles do not match the GO terms associated with differentially**
1276 **expressed mRNAs.**
1277 (A) Volcano plot of miRNA expression (red dots indicate differentially expressed miRNA) in *fhplk1*-RNAi
1278 juvenile *F. hepatica*. (B) Mean $\log_2$foldchange and frequency of GO terms for the predicted target
1279 transcripts of differentially expressed miRNAs following *fhplk1*-RNAi in *F. hepatica* juveniles.

1280 **S6 Fig. The PLK1 inhibitor BI 2536 does not affect *Fasciola hepatica* motility *in vitro*.**
1281 (A) Conservation of BI 2536 binding residues within *F. hepatica* FhPLK1, *Echinococcus multilocularis*
1282 EmPLK1, *Schistosoma mansoni* SmPLK1 and *Homo sapiens* PLK1 kinase domains, but not FhPLK2
1283 or FhPLK4 (residues implicated in BI 2536 binding highlighted in black; Leu_{132} residue critical to drug
1284 interaction in *H. sapiens* PLK1 highlighted in red and marked with a red arrow). (B) Worm motility (%)
1285 ±SEM of *F. hepatica* newly excysted juveniles (NEJs) 18 hours after *in vitro* BI 2536 treatment. (C)

1286 Motility profile of *F. hepatica* NEJs treated with 10 μM BI 2536 (blue), 0.1% DMSO (purple) and 1 μM
1287 TCBZ (green). Each line represents a single parasite; data presented as worm length (μm) over time
1288 (frames).

1289 **S1 Table. Summary table of predicated *Fasciola hepatica* kinome based on bioinformatic screen.**
1290 Genes IDs, BLAST hits, IDs in alternative *F. hepatica* genome assembly listed. Eukaryotic protein
1291 kinases and atypical protein kinases in separate sheets.

1292 **S2 Table. Summary of kinases downregulated following irradiation of *Fasciola hepatica***
1293 **juveniles and upregulated in faster-growing *in vivo F. hepatica* juveniles.**

1294 **S3 Table. DESeq2 results after three weeks of *fhplk1* RNAi in *Fasciola hepatica* juveniles *in vitro*.**
1295 (Sheet 1) Downregulated genes (adjp < 0.001), (Sheet 2) Upregulated genes (adjp < 0.001), (Sheet 3)
1296 All DESeq2 results.

1297 **S4 Table. Common downregulated genes following *fhplk1* RNAi in *Fasciola hepatica* juveniles,**
1298 **irradiation in *F. hepatica* juveniles and irradiation in *Schistosoma mansoni* adults.**
1299 (Sheet 1) Genes downregulated in both *fhplk1*-RNAi-*F. hepatica* juveniles, irradiated *F. hepatica*
1300 juveniles and irradiated *S. mansoni* adults. (Sheet 2) Genes downregulated in both irradiated *F. hepatica*
1301 juveniles and irradiated *S. mansoni* adults. (Sheet 3) Genes downregulated in both *fhplk1*-RNAi-*F.*
1302 *hepatica* juveniles and irradiated *S. mansoni* adults. (Sheet 4) Genes downregulated in both *fhplk1*-
1303 RNAi-*F. hepatica* juveniles and irradiated *F. hepatica* juveniles.

1304 **S5 Table. Log_2FoldChange of predicted *Fasciola hepatica* neuropeptides following RNAi of**
1305 ***fhplk1* in juveniles across three weeks *in vitro*.**

1306 **S6 Table. Shared genes that are upregulated following *fhplk1* RNAi and downregulated in faster-**
1307 **growing *in vivo* juveniles.**

1308 **S7 Table. Comparison of fold change for signalling-associated genes following *fhplk1* RNAi or**
1309 **in faster-growing *in vivo* juveniles.**

1310 **S8 Table. GO terms upregulated in adult *Schistosoma mansoni* following neoblast-like cell**
1311 **ablation.**
1312 (Sheet 1) GO terms upregulated 14 days after irradiation. (Sheet 2) GO terms upregulated 21 days after
1313 *smh2b* RNAi. (Sheet 3) GO terms upregulated 21 days after *smfgfrA* RNAi.

1314 **S9 Table. Differentially expressed miRNAs following *fhplk1* RNAi in *Fasciola hepatica* juveniles.**
1315 (Sheet 1) Differentially expressed miRNAs. (Sheet 2) Predicted targets of differentially expressed
1316 miRNAs.

1317 **S10 Table. Primers used in PCR reactions.**

1318 **S11 Table. Raw values used to produce graphs in Figs 1, 3, 4, 5, 6, S1, S2, S3, S4 and S6.**

1319 **S1 File. Fasta file of all sequences in predicted *Fasciola hepatica* kinome**

1320 **S2 File. Nucleotide sequences of 'novel' MSTRG *Fasciola hepatica* transcripts identified by**
1321 **Stringtie during transcriptomic processing.**

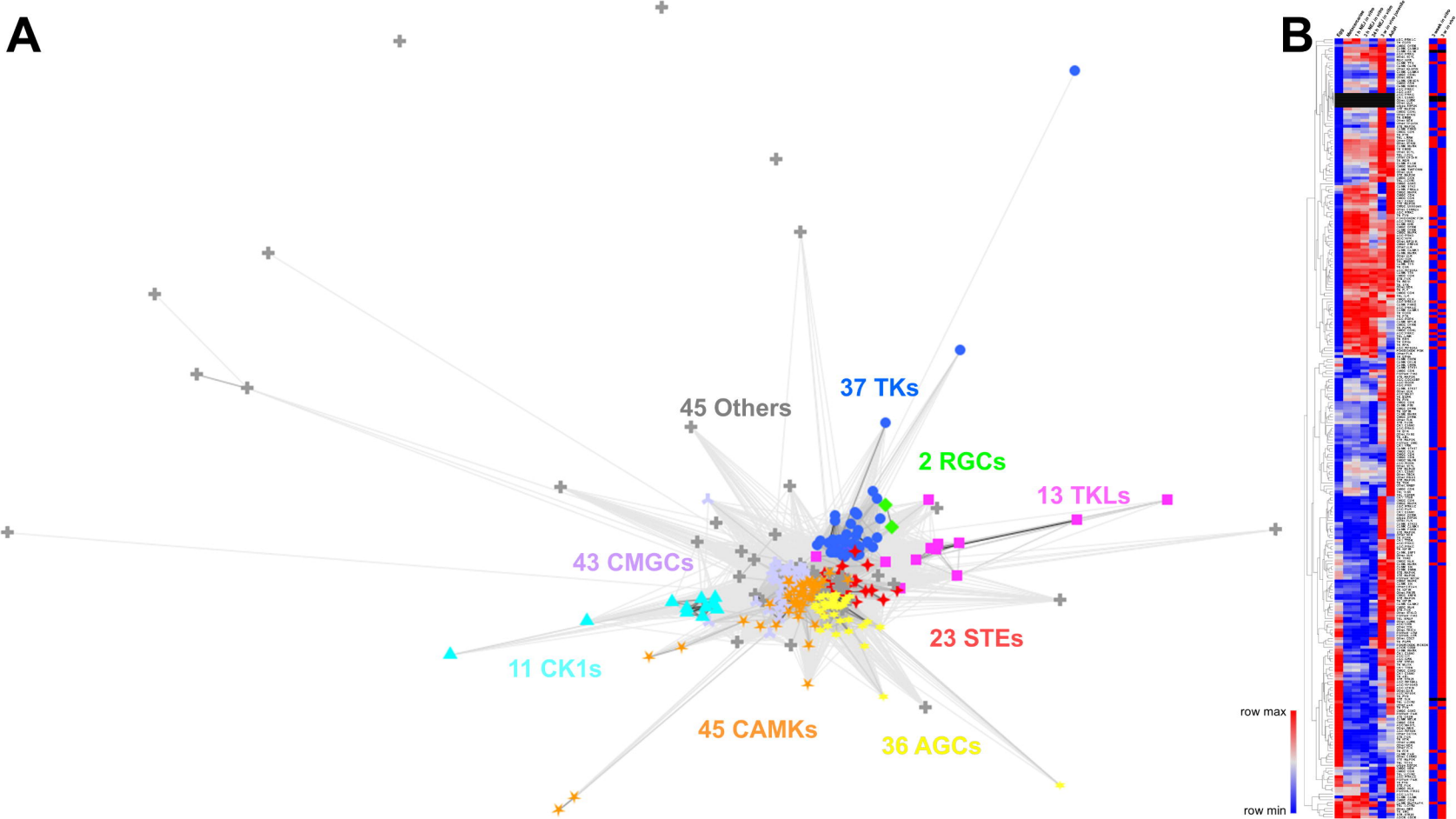
A
B
45 Others
37 TKs
2 RGCs
13 TKLs
43 CMGCs
23 STEs
11 CK1s
45 CAMKs
36 AGCs
row max
row min

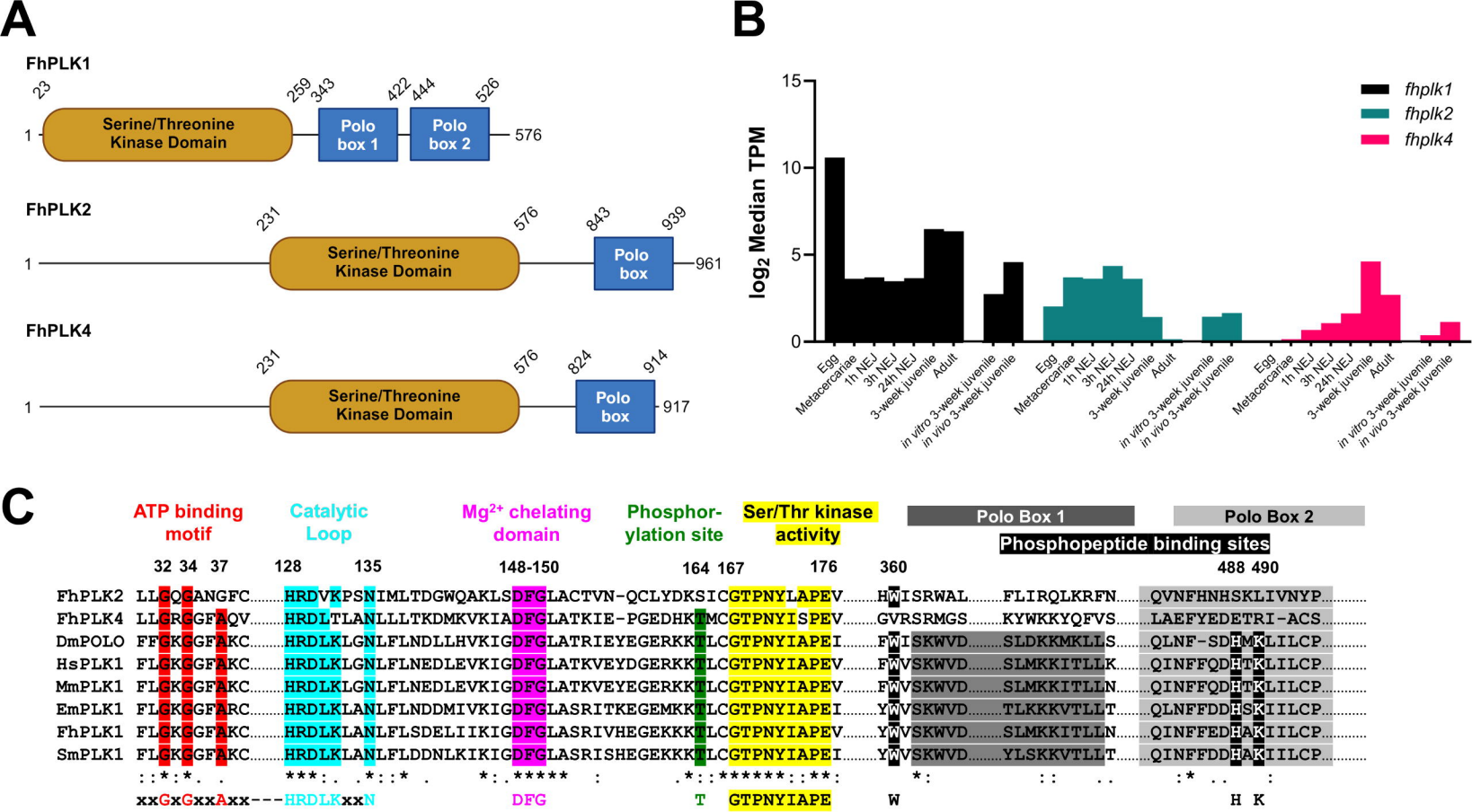
A
FhPLK1
23
259
343
422
444
526
1
Serine/Threonine Kinase Domain
Polo box 1
Polo box 2
576
FhPLK2
231
576
843
939
1
Serine/Threonine Kinase Domain
Polo box
961
FhPLK4
231
576
824
914
1
Serine/Threonine Kinase Domain
Polo box
917
B
log2 Median TPM
15
10
5
0
fhplk1
fhplk2
fhplk4
Egg
Metacercariae
1h NEJ
3h NEJ
24h NEJ
3-week juvenile
Adult
in vitro 3-week juvenile
in vivo 3-week juvenile
C
ATP binding motif
Catalytic Loop
Mg2+ chelating domain
Phosphor-ylation site
Ser/Thr kinase activity
Polo Box 1
Polo Box 2
Phosphopeptide binding sites
32 34 37
128
135
148-150
164 167
176
360
488 490
FhPLK2 LLGQGANGFC HRDVKPSNIMLTDGWQAKLSDFGLACTVN-QCLYDKSICGTPNYLAPEV HWISRWAL FLIRQLKRFN QVNFHNHSKLIVNYP
FhPLK4 LLGRGGFAQV HRDLTLANLLLTKDMKVKIADFGLATKIE-PGEDHKIMCGTPNYISPEV GVRSRMGS KYWKKYQFVS LAEFYEDETRI-ACS
DmPOLO FFGKGGFAKC HRDLKLGNLFLNDLLHVKIGDFGLATRIEYEGERKKILCGTPNYIAPEI FWISKWVD SLDKKMKLLS QLNF-SDHMKLILCP
HsPLK1 FLGKGGFAKC HRDLKLGNLFLNEDLEVKIGDFGLATKVEYDGERKKILCGTPNYIAPEV FWVSKWVD SLMKKITLLK QINFFQDHTKLILCP
MmPLK1 FLGKGGFAKC HRDLKLGNLFLNEDLEVKIGDFGLATKVEYEGERKKILCGTPNYIAPEV FWVSKWVD SLMKKITLLN QINFFQDHTKLILCP
EmPLK1 FLGKGGFARC HRDLKLANLFLNDDMIVKIGDFGLASRITKEGEMKKILCGTPNYIAPEI YWVSKWVD TLKKKVTLLT QLNFFDDHSKIILCP
FhPLK1 FLGKGGFAKC HRDLKLANLFLSDELIIKIGDFGLASRIVHEGEKKKILCGTPNYIAPEV YWVSKWVD SLMKKITLLN QINFFEDHAKIILCP
SmPLK1 FLGKGGFAKC HRDLKLANLFLDDNLKIKIGDFGLASRISHEGEKKKILCGTPNYIAPEI YWVSKWVD YLSKKVTLLT QINFFDDHAKIILCP
::*:*. . ***:. .*::* . *:.***** : .*::******:**: *: :: .. :* .. :
xxGxGxxAxx---HRDLKxxN DFG T GTPNYIAPE W H K

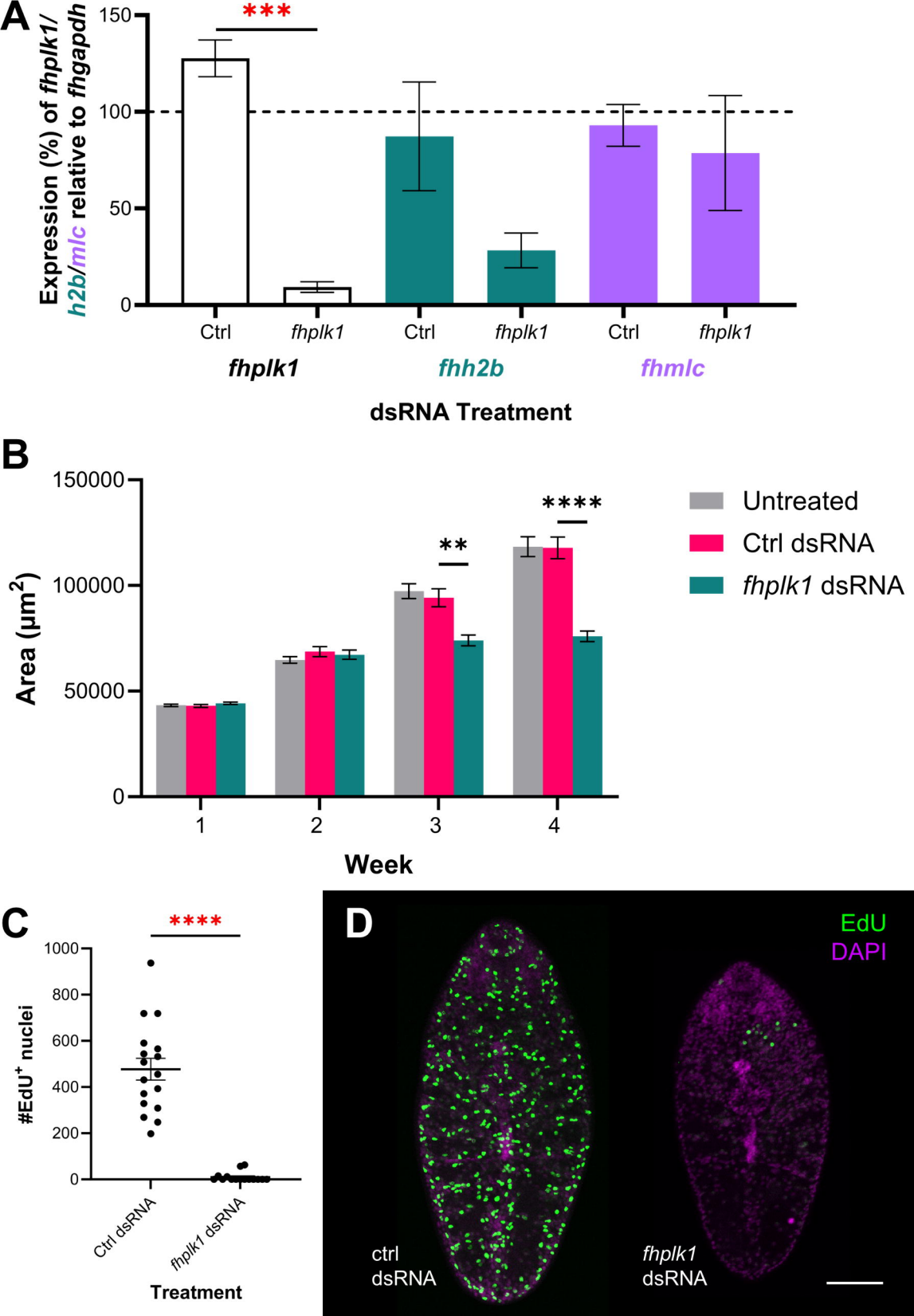
A
Expression (%) of fhplk1/h2b/mlc relative to fhgapdh
150
100
50
0
***
Ctrl
fhplk1
Ctrl
fhplk1
Ctrl
fhplk1
fhplk1
fhh2b
fhmlc
dsRNA Treatment
B
Area (µm²)
150000
100000
50000
0
**
****
1
2
3
4
Week
Untreated
Ctrl dsRNA
fhplk1 dsRNA
C
#EdU⁺ nuclei
1000
800
600
400
200
0
****
Ctrl dsRNA
fhplk1 dsRNA
Treatment
D
EdU
DAPI
ctrl
dsRNA
fhplk1
dsRNA

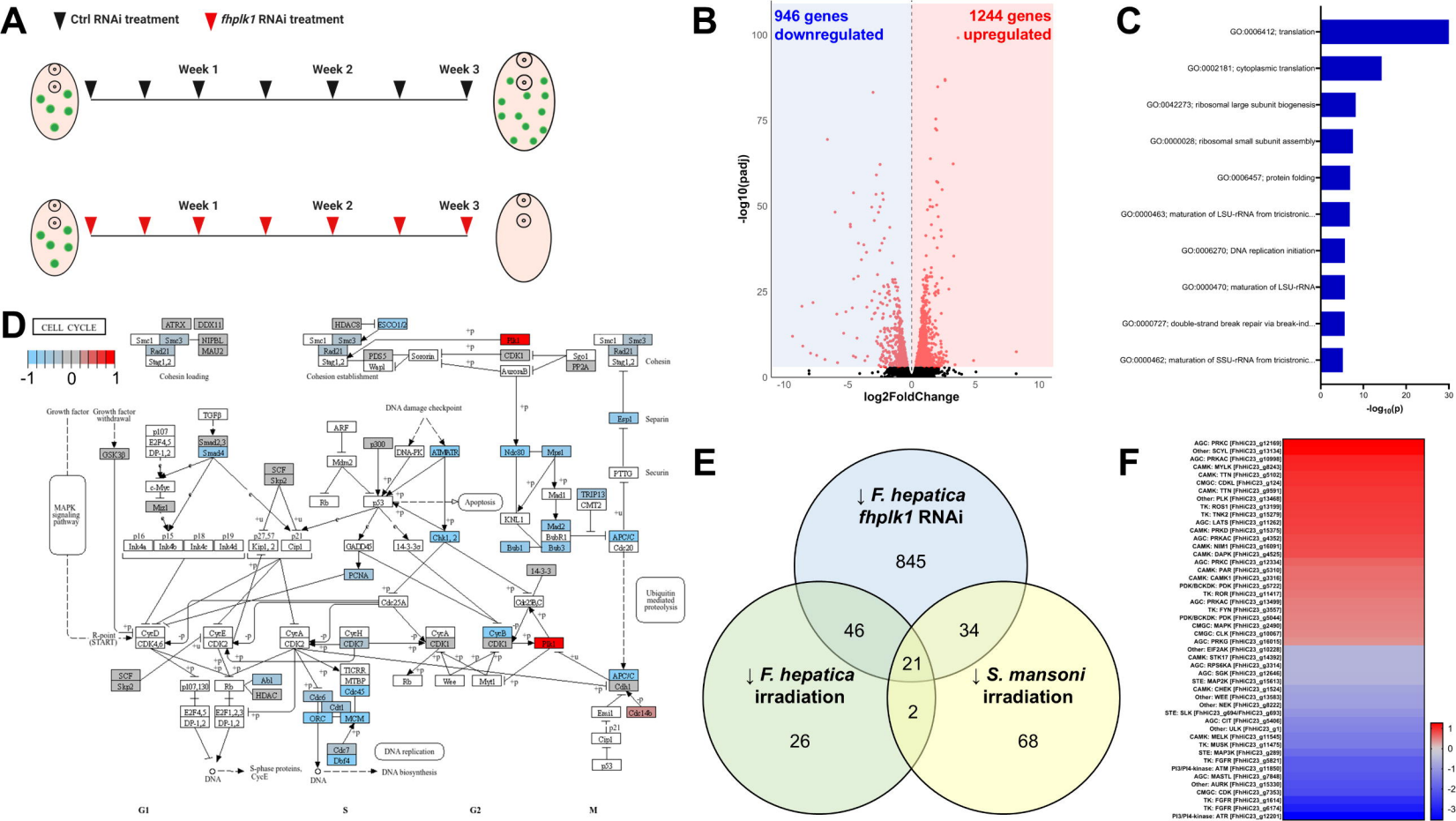
A
Ctrl RNAi treatment
fhplk1 RNAi treatment
Week 1
Week 2
Week 3
B
946 genes downregulated
1244 genes upregulated
-log10(padj)
log2FoldChange
C
GO:0006412; translation
GO:0002181; cytoplasmic translation
GO:0042273; ribosomal large subunit biogenesis
GO:0000028; ribosomal small subunit assembly
GO:0006457; protein folding
GO:0000463; maturation of LSU-rRNA from tricistronic...
GO:0006270; DNA replication initiation
GO:0000470; maturation of LSU-rRNA
GO:0000727; double-strand break repair via break-ind...
GO:0000462; maturation of SSU-rRNA from tricistronic...
-log10(p)
D
CELL CYCLE
Cohesin loading
Cohesin establishment
Cohesin
Separin
Securin
DNA damage checkpoint
Apoptosis
Ubiquitin mediated proteolysis
DNA replication
DNA biosynthesis
S-phase proteins, CycE
G1
S
G2
M
E
↓ F. hepatica fhplk1 RNAi
845
46
34
21
2
↓ F. hepatica irradiation
26
↓ S. mansoni irradiation
68
F

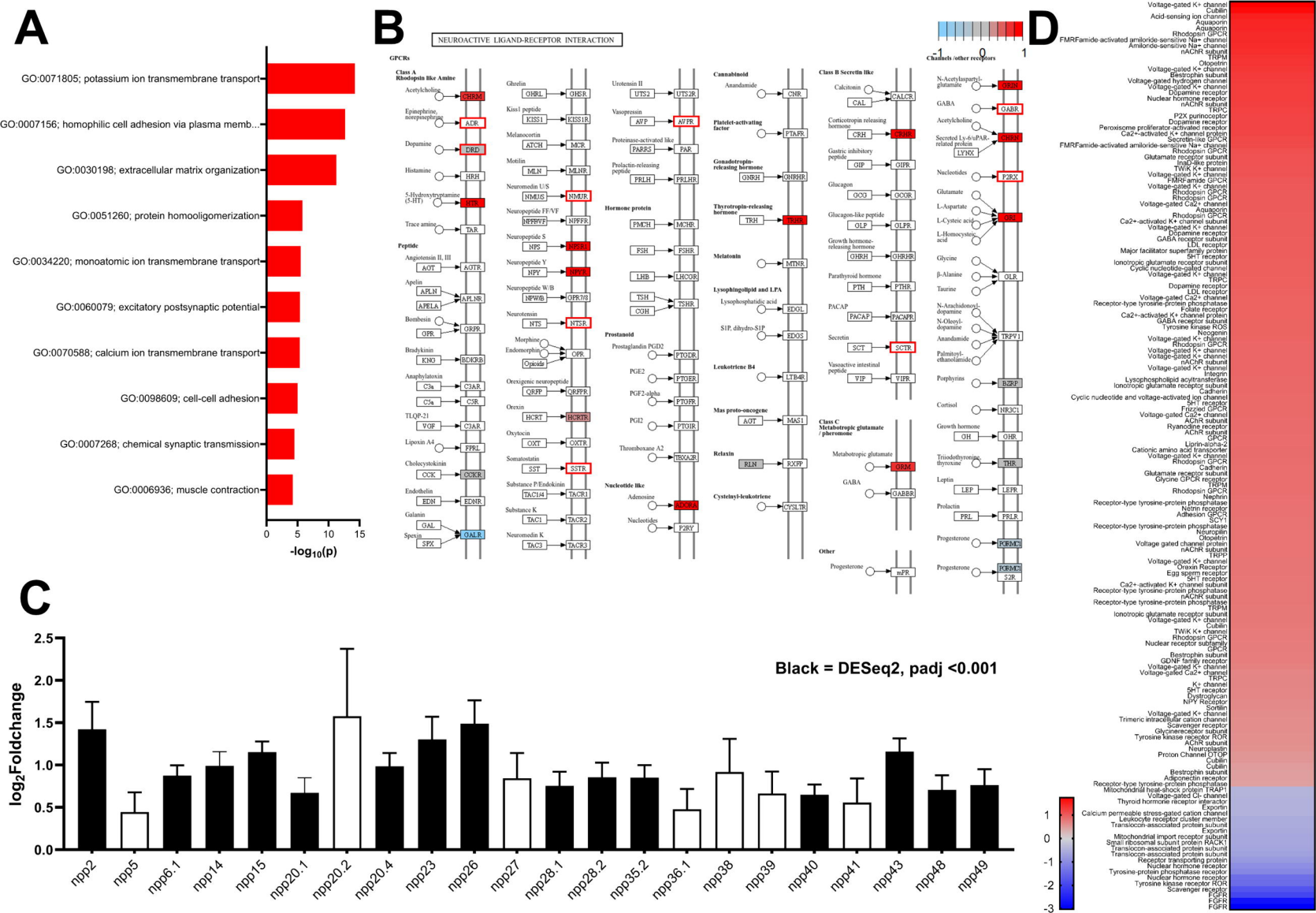
A
GO:0071805; potassium ion transmembrane transport
GO:0007156; homophilic cell adhesion via plasma memb...
GO:0030198; extracellular matrix organization
GO:0051260; protein homooligomerization
GO:0034220; monoatomic ion transmembrane transport
GO:0060079; excitatory postsynaptic potential
GO:0070588; calcium ion transmembrane transport
GO:0098609; cell-cell adhesion
GO:0007268; chemical synaptic transmission
GO:0006936; muscle contraction
0
5
10
15
-log10(p)
B
NEUROACTIVE LIGAND-RECEPTOR INTERACTION
GPCRs
Class A Rhodopsin like Amine
Acetylcholine
CHRM1
Epinephrine, norepinephrine
ADR
Dopamine
DRD
Histamine
HRH
5-Hydroxytryptamine (5-HT)
HTR
Trace amine
TAR
Peptide
Angiotensin II, III
AGT
AGTR
Apelin
APLN
APELA
APLNR
Bombesin
GPR
GRPR
Bradykinin
KNG
BDKRB
Anaphylatoxin
C3a
C3AR
C5a
C5R
TLQP-21
VGF
C3AR
Lipoxin A4
FPRL
Cholecystokinin
CCK
CCKR
Endothelin
EDN
EDNR
Galanin
GAL
Spexin
SPX
GALR
Ghrelin
GHRL
GHSR
Kiss1 peptide
KISS1
KISS1R
Melanocortin
ATCH
MCR
Motilin
MLN
MLNR
Neuromedin U/S
NMU/S
NMUR
Neuropeptide FF/VF
NPFF/VF
NPFFR
Neuropeptide S
NPS
NPSR1
Neuropeptide Y
NPY
NPY1R
Neuropeptide W/B
NPW/B
GPR7/8
Neurotensin
NTS
NTSR
Morphine
Endomorphin
Opioids
OPR
Orexigenic neuropeptide
QRFP
QRFPR
Orexin
HCRT
HCRTR
Oxytocin
OXT
OXTR
Somatostatin
SST
SSTR
Substance P/Endokinin
TAC1/4
TACR1
Substance K
TAC1
TACR2
Neuromedin K
TAC3
TACR3
Urotensin II
UTS2
UTS2R
Vasopressin
AVP
AVPR
Proteinase-activated like
PARRS
PAR
Prolactin-releasing peptide
PRLH
PRLHR
Hormone protein
FMCH
MCHR
FSH
FSHR
LHB
LHCGR
TSH
TSHR
CGH
Prostanoid
Prostaglandin PGD2
PTGDR
PGE2
PTGER
PGF2-alpha
PTGFR
PGI2
PTGIR
Thromboxane A2
TBXA2R
Nucleotide like
Adenosine
ADORA
Nucleotides
P2RY
Cannabinoid
Anandamide
CNR
Platelet-activating factor
PTAFR
Gonadotropin-releasing hormone
GNRH
GNRHR
Thyrotropin-releasing hormone
TRH
TRHR
Melatonin
MTNR
Lysophingolipid and LPA
Lysophosphatidic acid
EDGL
S1P, dihydro-S1P
EDGS
Leukotriene B4
LTB4R
Mas proto-oncogene
AGT
MAS1
Relaxin
RLN
RXFP
Cysteinyl-leukotriene
CYSLTR
Class B Secretin like
Calcitonin
CAL
CALCR
Corticotropin releasing hormone
CRH
CRHR
Gastric inhibitory peptide
GIP
GIPR
Glucagon
GCG
GCGR
Glucagon-like peptide
GLP
GLPR
Growth hormone-releasing hormone
GHRH
GHRHR
Parathyroid hormone
PTH
PTHR
PACAP
PACAP
PACAPR
Secretin
SCT
SCTR
Vasoactive intestinal peptide
VIP
VIPR
Class C Metabotropic glutamate / pheromone
Metabotropic glutamate
GRM
GABA
GABBR
Other
Progesterone
mPR
-1
0
1
Channels /other receptors
N-Acetylaspartyl-glutamate
GRIN
GABA
GABR
Acetylcholine
CHRN
Secreted Ly-6/uPAR-related protein
LYNX
Nucleotides
P2RX
Glutamate
L-Aspartate
L-Cysteic acid
L-Homocysteic acid
GRIK
Glycine
β-Alanine
Taurine
GLR
N-Arachidonoyl-dopamine
N-Oleoyl-dopamine
Anandamide
Palmitoyl-ethanolamide
TRPV1
Porphyrins
BZRP
Cortisol
NR3C1
Growth hormone
GH
GHR
Triiodothyronine, thyroxine
THR
Leptin
LEP
LEPR
Prolactin
PRL
PRLR
Progesterone
PGRMC1
Progesterone
PGRMC2
S2R
C
Black = DESeq2, padj <0.001
log2Foldchange
2.5
2.0
1.5
1.0
0.5
0.0
npp2
npp5
npp6.1
npp14
npp15
npp20.1
npp20.2
npp20.4
npp23
npp26
npp27
npp28.1
npp28.2
npp35.2
npp36.1
npp38
npp39
npp40
npp41
npp43
npp48
npp49
D
Voltage-gated K+ channel
Cubilin
Acid-sensing ion channel
Aquaporin
Aquaporin
Rhodopsin GPCR
FMRFamide-activated amiloride-sensitive Na+ channel
Amiloride-sensitive Na+ channel
nAChR subunit
TRPM
Otopetrin
Voltage-gated K+ channel
Bestrophin subunit
Voltage-gated hydrogen channel
Voltage-gated K+ channel
Dopamine receptor
Nuclear hormone receptor
nAChR subunit
TRPC
P2X purinoceptor
Dopamine receptor
Peroxisome proliferator-activated receptor
Ca2+-activated K+ channel protein
Secretin-like GPCR
FMRFamide-activated amiloride-sensitive Na+ channel
Rhodopsin GPCR
Glutamate receptor subunit
IsaK2-like protein
TWIK K+ channel
Voltage-gated K+ channel
FMRFamide GPCR
Voltage-gated K+ channel
Rhodopsin GPCR
Rhodopsin GPCR
Voltage-gated Ca2+ channel
Aquaporin
Rhodopsin GPCR
Ca2+-activated K+ channel subunit
Voltage-gated K+ channel
Dopamine receptor
GABA receptor subunit
LDL receptor
Major facilitator superfamily protein
5HT receptor
Ionotropic glutamate receptor subunit
Cyclic nucleotide-gated channel
Voltage-gated K+ channel
TRPC
Dopamine receptor
LDL receptor
Voltage-gated Ca2+ channel
Receptor-type tyrosine-protein phosphatase
Folate receptor
Ca2+-activated K+ channel protein
GABA receptor subunit
Tyrosine kinase ROS
Neogenin
Voltage-gated K+ channel
Rhodopsin GPCR
Voltage-gated K+ channel
Voltage-gated K+ channel
nAChR subunit
Voltage-gated K+ channel
Integrin
Lysophospholipid acyltransferase
Ionotropic glutamate receptor subunit
Cadherin
Cyclic nucleotide and voltage-activated ion channel
5HT receptor
Frizzled GPCR
Voltage-gated Ca2+ channel
AChR subunit
Ryanodine receptor
AChR subunit
GPCR
Liprin-alpha-2
Cationic amino acid transporter
Voltage-gated K+ channel
Rhodopsin GPCR
Cadherin
Glutamate receptor subunit
Glycine GPCR receptor
TRPM
Rhodopsin GPCR
Nephrin
Receptor-type tyrosine-protein phosphatase
Netrin receptor
Adhesion GPCR
SCY1
Receptor-type tyrosine-protein phosphatase
Neuropilin
Otopetrin
Voltage gated channel protein
nAChR subunit
TRPP
Voltage-gated K+ channel
Orexin Receptor
Egg sperm receptor
5HT receptor
Ca2+-activated K+ channel subunit
Receptor-type tyrosine-protein phosphatase
nAChR subunit
Receptor-type tyrosine-protein phosphatase
TRPM
Ionotropic glutamate receptor subunit
Voltage-gated K+ channel
Cubilin
TWIK K+ channel
Rhodopsin GPCR
Nuclear receptor subfamily
GPCR
Bestrophin subunit
GDNF family receptor
Voltage-gated K+ channel
Voltage-gated Ca2+ channel
TRPC
K+ channel
5HT receptor
Dystroglycan
NPY Receptor
Sortilin
Voltage-gated K+ channel
Trimeric intracellular cation channel
Scavenger receptor
Glycinereceptor subunit
Tyrosine kinase receptor ROR
AChR subunit
Neuroplastin
Proton Channel DTOP
Cubilin
Cubilin
Bestrophin subunit
Adiponectin receptor
Receptor-type tyrosine-protein phosphatase
Mitochondrial heat-shock protein TRAP1
Voltage-gated Cl- channel
Thyroid hormone receptor interactor
Exportin
Calcium permeable stress-gated cation channel
Leukocyte receptor cluster member
Translocon-associated protein subunit
Exportin
Mitochondrial import receptor subunit
Small ribosomal subunit protein RACK1
Translocon-associated protein subunit
Translocon-associated protein subunit
Receptor transporting protein
Nuclear hormone receptor
Tyrosine-protein phosphatase receptor
Nuclear hormone receptor
Tyrosine kinase receptor ROR
Scavenger receptor
FGFR
FGFR
FGFR
1
0
-1
-2
-3

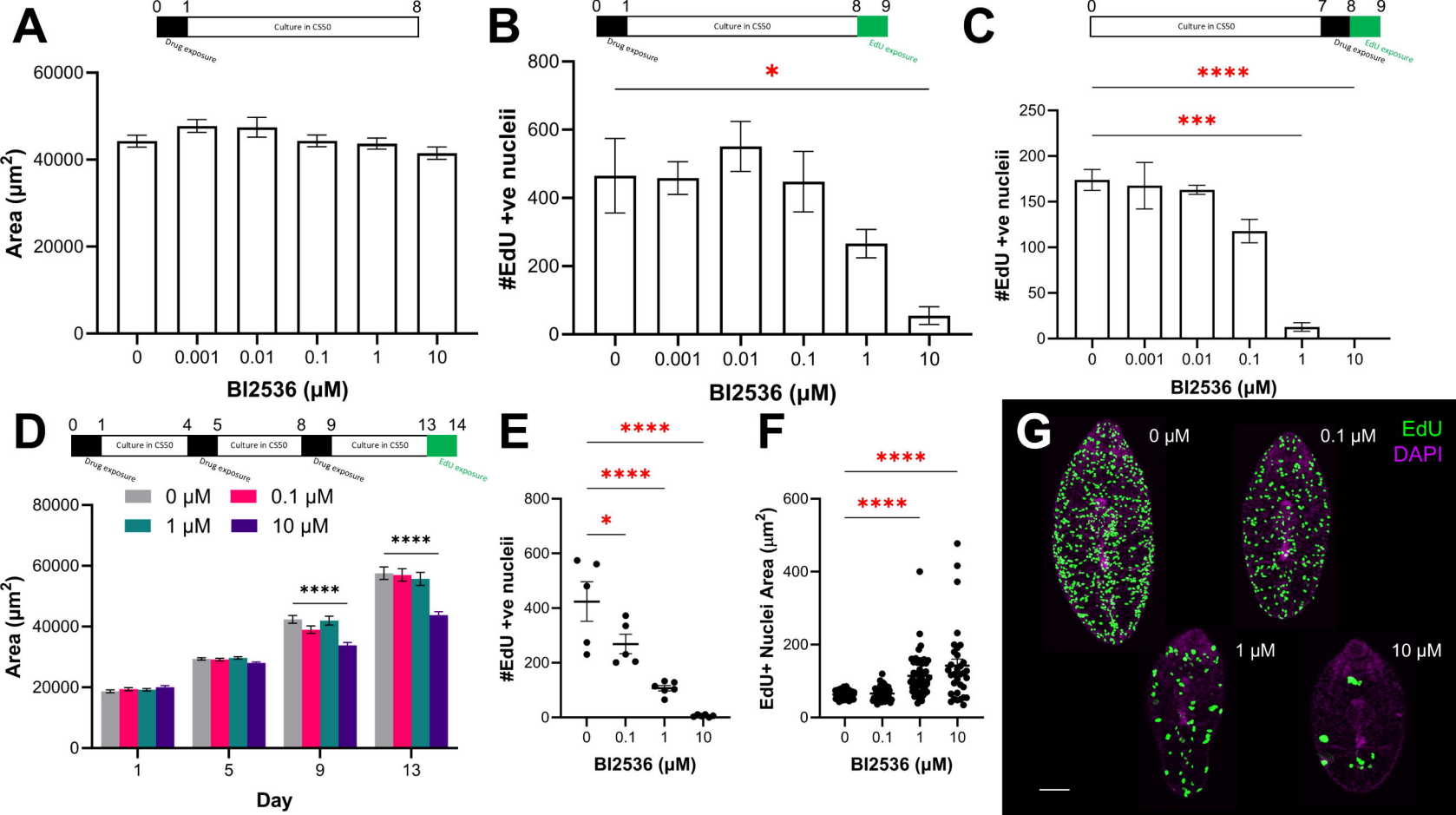
A
0 1 8
Culture in CS50
Drug exposure
Area (μm²)
60000
40000
20000
0
0 0.001 0.01 0.1 1 10
BI2536 (μM)
B
0 1 8 9
Culture in CS50
Drug exposure
EdU exposure
#EdU +ve nucleii
800
600
400
200
0
*
0 0.001 0.01 0.1 1 10
BI2536 (μM)
C
0 7 8 9
Culture in CS50
Drug exposure
EdU exposure
#EdU +ve nucleii
250
200
150
100
50
0
****
***
0 0.001 0.01 0.1 1 10
BI2536 (μM)
D
0 1 4 5 8 9 13 14
Culture in CS50
Drug exposure
EdU exposure
0 μM
0.1 μM
1 μM
10 μM
Area (μm²)
80000
60000
40000
20000
0
****
****
1 5 9 13
Day
E
#EdU +ve nucleii
800
600
400
200
0
****
****
*
0 0.1 1 10
BI2536 (μM)
F
EdU+ Nuclei Area (μm²)
600
400
200
0
****
****
0 0.1 1 10
BI2536 (μM)
G
0 μM
0.1 μM
1 μM
10 μM
EdU
DAPI